



Contents lists available at ScienceDirect



## Tectonophysics

journal homepage: [www.elsevier.com/locate/tecto](http://www.elsevier.com/locate/tecto)

# Zircon U-Pb and Hf isotopic constraints from eastern Transhimalayan batholiths on the precollisional magmatic and tectonic evolution in southern Tibet

Han-Yi Chiu <sup>a</sup>, Sun-Lin Chung <sup>a,\*</sup>, Fu-Yuan Wu <sup>b</sup>, Dunyi Liu <sup>c</sup>, Yu-Hsuan Liang <sup>a</sup>, I-Jhen Lin <sup>a</sup>, Yoshiyuki Izuka <sup>d</sup>, Lie-Wen Xie <sup>b</sup>, Yanbin Wang <sup>c</sup>, Mei-Fei Chu <sup>a</sup>

<sup>a</sup> Department of Geosciences, National Taiwan University, Taipei 106, Taiwan<sup>b</sup> Institute of Geology and Geophysics, Chinese Academy of Sciences, Beijing 100029, China<sup>c</sup> Institute of Geology, Chinese Academy of Geological Sciences, Beijing 100037, China<sup>d</sup> Institute of Earth Sciences, Academia Sinica, Taipei 115, Taiwan

## ARTICLE INFO

## Article history:

Received 1 May 2008

Received in revised form 15 January 2009

Accepted 23 February 2009

Available online xxxx

## Keywords:

Zircon  
U-Pb and Hf isotope  
Tethyan subduction  
Transhimalayan batholiths  
Tibet  
Tectonic evolution

## ABSTRACT

Before the Indian collision with Asia, northward subduction of the Neo-Tethyan oceanic lithosphere produced an Andean-type convergent margin in South Asia characterized by arc magmatism starting from the early Jurassic and lasting until the Eocene. The magmatic arc is now represented by widespread intrusive bodies or the so-called Transhimalayan batholiths in the Lhasa terrane of southern Tibet that have been divided into two main magmatic suites, i.e., the northern plutonic belt and the southern Gangdese Batholith. Their temporal distribution, concerning how exactly the magmatic suites correlate eastwards and then southeastwards around the eastern Himalayan syntaxis, however, remains poorly constrained. Here we report the first combined zircon U-Pb and Hf isotopic study of the Transhimalayan batholiths from the eastern part of the Lhasa terrane ( $\sim 95\text{--}97.5^{\circ}\text{E}$  and  $\sim 28.5\text{--}30^{\circ}\text{N}$ ), SE Tibet. Zircon U-Pb dating results of 24 granitoids indicate that the rocks were emplaced principally in the Early Cretaceous ( $\sim 133\text{--}110$  Ma) and subordinately in the Paleocene ( $\sim 66\text{--}57$  Ma), long after an older granite intrusion in the earliest Jurassic ( $\sim 198$  Ma). The zircon  $\epsilon_{\text{Hf}}(T)$  values range from +5 to -20, yielding Hf crustal model ages ( $T_{\text{DM}}$ ) between 0.8 and 2.4 Ga that peak at  $\sim 1.7$  Ga, suggesting a major episode of crustal growth in the Proterozoic and a predominantly, or even exclusively, crustal source for the granitoid petrogenesis. These zircon U-Pb and Hf isotopic constraints, together with whole-rock geochemical characteristics, allow us to correlate them to S-type granitoids in the northern plutonic belt, rather than to the I-type Gangdese Batholith from the central part of the southern Lhasa terrane. In contrast to the Gangdese magmatism that formed with a significant juvenile mantle input related to the Neo-Tethyan subduction, these S-type granitoids show geochemical similarities to the North American Cordilleran Interior batholiths that did not form directly from a subduction setting. Thus, we attribute the petrogenesis of the widespread Early Cretaceous granitoids in the northern belt and eastern Himalayan batholiths to a postcollisional regime due to the Late Jurassic-Early Cretaceous continental collision between the Lhasa and Qiangtang terranes. Under this framework, the S-type magmatism was generated in response to collision-induced crustal thickening, which may have capabilities of causing crustal anatexis by itself in the region. However, continued interplay with the Neo-Tethyan subduction zone processes such as back-arc extension could also have played a crucial, and long-lasting, role in the magma generation.

© 2009 Elsevier B.V. All rights reserved.

## 1. Introduction

In southern Tibet, the elongated belt of granitoids that occurs in the Lhasa terrane north of the Yarlu-Tsangpo suture (Fig. 1) has been termed the "Transhimalayan batholiths" (Searle et al., 1987; for review and references therein) and widely regarded as a major component of the Andean-type continental margin along South Asia resulting from northward subduction of the Neo-Tethyan oceanic lithosphere before India started colliding with Asia (e.g., Allègre et al., 1984; Debon et al., 1986; Searle et al., 1987; Harris et al., 1988; Yin and Harrison, 2000;

Chung et al., 2005; Kapp et al., 2005a; Mo et al., 2005; Wen et al., 2008a). Knowledge about the precollisional history in this region, however, remains limited because previous studies mostly concentrated on issues of postcollisional geology in particular those related to uplift of the Tibetan plateaus and surrounding mountain ranges.

As part of a systematic study of the precollisional Transhimalayan magmatism (Chu et al., 2006; Lee et al., 2007, this volume; Liang et al., 2008; Wen et al., 2008a, 2008b), this paper reports for the first time a combined in-situ analysis of zircon U-Pb ages and Lu-Hf isotopes for the eastern Transhimalayan batholiths, emplaced in the easternmost part of the Lhasa terrane, the southeastern Tibetan plateau (Fig. 1). The results significantly improve our understanding of the age distribution and geochemical characteristics of the eastern Transhimalayan batholiths,

\* Corresponding author.

E-mail address: [sunlin@ntu.edu.tw](mailto:sunlin@ntu.edu.tw) (S.-L. Chung).

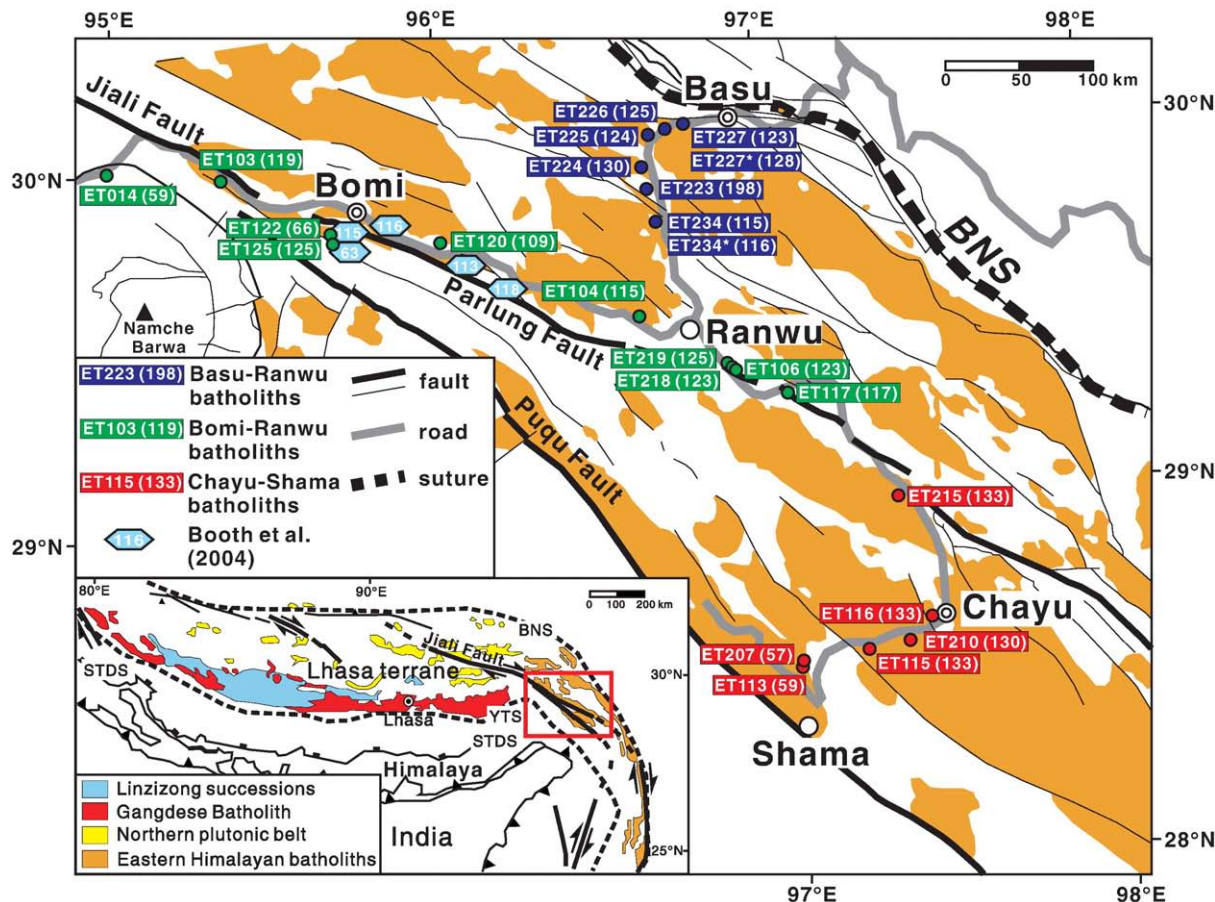


**Fig. 1.** Simplified geological map showing the sample localities and distribution of major intrusive bodies in the eastern Lhasa terrane, SE Tibet (Pan et al., 2004). New zircon U-Pb age results conducted by this paper and those reported by Booth et al. (2004) are given in the parentheses and hexagons, respectively (numbers in Ma). BNS—Bangong–Nujiang suture; YTS—Yarlu–Tsangpo suture; STDS—South Tibet Detachment System.

which, together with our comparative studies from the central part of the Lhasa terrane, shed new insights into not only the magmatic but also tectonic evolution in southern Tibet before the India-Asia collision.

## 2. Background and samples

The Lhasa terrane is widely believed to have dispersed from Gondwana during the Permian or Triassic (Allègre et al., 1984; Chang et al., 1986), then drifted northward and finally collided with the Qiangtang terrane during the Late Jurassic–Early Cretaceous (Kapp et al., 2005a). The terrane is bordered by the Bangong–Nujiang suture in north and by the Yarlu–Tsangpo suture in south (Fig. 1), with the latter resulting from closure of the Neo-Tethys ocean owing to the continental collision between India and Asia (Yin and Harrison, 2000). The Transhimalayan batholiths, distributing for a distance of ~2500 km in the Lhasa terrane, have been divided into two principal magmatic suites: (1) a southern Gangdese belt represented by the gigantic Gangdese Batholith that consists dominantly of Late Cretaceous to Eocene granotoids with I-type geochemical composition (Debon et al., 1986; Searle et al., 1987; Wen et al., 2008a), and (2) a northern plutonic belt of peraluminous or S-type granitoids such as those exposed in the Nyainqntanglha Range that were emplaced largely in the Early Cretaceous (Xu et al., 1985; Harris et al., 1990; Kapp et al., 2005b).

It is generally thought that the Gangdese Batholith, and associated Linzizong volcanic successions (Fig. 1), are the magmatic products by northward subduction of the Neo-Tethyan oceanic lithosphere under

South Asia. However, the petrogenesis of the northern plutonic belt remains an issue of debates and different models have been proposed, including: (1) crustal anatexis during and/or postdating the continental collision between the Lhasa and Qiangtang terranes (Xu et al., 1985; Pearce and Mei, 1988), (2) high-temperature crustal melting due to upwelling of the asthenosphere after the Lhasa–Qiangtang collision (Harris et al., 1990), and (3) a low-angle, or “shallow,” subduction of the Neo-Tethyan oceanic lithosphere (Coulon et al., 1986; Ding et al., 2003; Zhang et al., 2004; Kapp et al., 2005a; Chu et al., 2006). Besides, how these magmatic belts correlate to the east, and then southeastwards around the eastern Himalayan syntaxis, the answer is uncertain because there have been few studies on the eastern Transhimalayan batholiths east of 95°E since the pioneering works carried out in the late seventies (Tu et al., 1982).

Therefore, we conducted field excursions along the main roads in the area from Bomi to Basu and Chayu (Shama), between  $\sim 95\text{--}97.5^{\circ}\text{E}$  and  $\sim 30\text{--}28.5^{\circ}\text{N}$ , SE Tibet (Fig. 1), through which 80+ granitoids of the eastern Transhimalayan batholiths were recovered for detailed petrochemical analyses (e.g., Lin et al., 2007). The granitoids are generally fresh looking and composed mainly of median-grained monzogranites, granodiorites and granites that contain rather simple mineral constituents including K-feldspar ( $\sim 40\%$ ), plagioclase ( $\sim 30\%$ ), quartz ( $\sim 20\%$ ), biotite ( $\sim 5\text{--}10\%$ ) and accessory minerals such as hornblende, muscovite, apatite and opaque phases. 24 among the samples were subjected to in-situ zircon U-Pb and Hf isotopic determination by this study. For the convenience, we divide the northwest-southeast-trending Transhimalayan batholiths in this

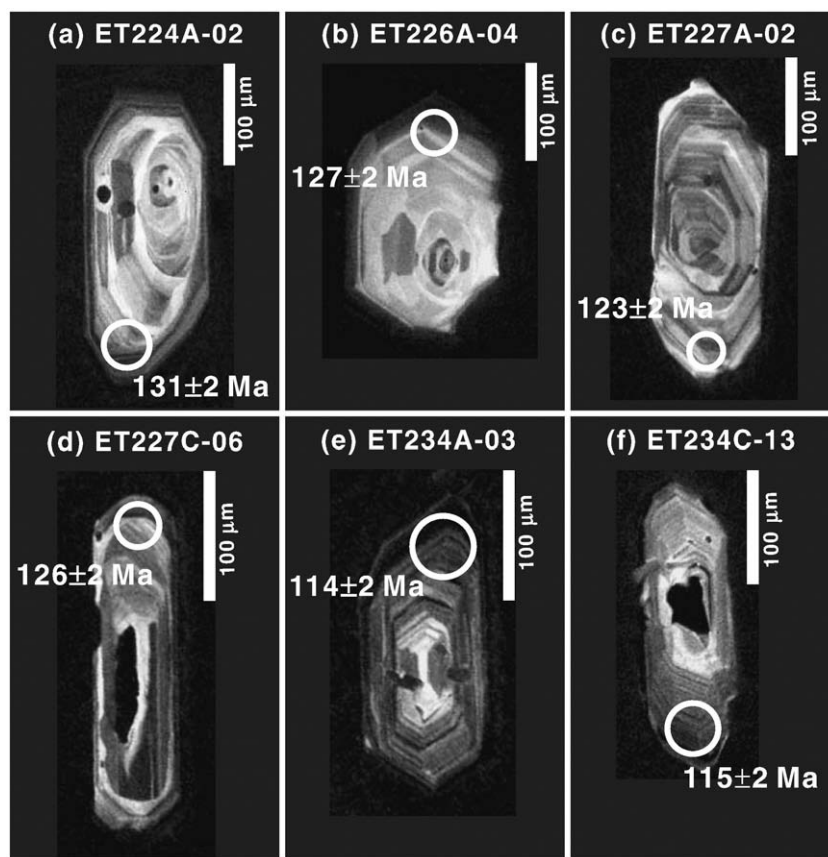


**Fig. 2.** Cathodoluminescence (CL) images of representative zircons separate from the studied samples. Circles indicate the positions of LA-ICPMS U-Pb age analyses, sizing 30–50  $\mu\text{m}$ . LA-MC-ICPMS Hf isotope analyses were performed on the same positions with a slightly larger, ~50–65  $\mu\text{m}$ , laser beam size.

region into three groups, namely, from north to south, the Basu–Ranwu, Bomi–Ranwu and Chayu–Shama batholiths (Fig. 1).

### 3. Analytical methods

Zircons were separated from ~3 kg samples using conventional heavy-liquid and magnetic separation techniques. Cathodoluminescence (CL) images (Fig. 2) were taken at the Institute of Earth Sciences, Academia Sinica, Taipei for examining the internal structures of individual zircon grains and selecting suitable positions for U-Pb and Lu-Hf isotope determinations.

#### 3.1. Zircon U-Pb geochronology

Zircon U-Pb isotopic analyses were performed using two analytical methods, the sensitive high-resolution ion microprobe (SHRIMP) and the laser ablation-inductively coupled plasma-mass spectrometry (LA-ICPMS). These include 10 age results that were obtained using the SHRIMP II equipped at the Beijing SHRIMP Center, Institute of Geology, Chinese Academy of Geological Sciences and reported in Liang et al. (2008) for tracing the source provenances of the Irrawaddy detrital zircons, and 14 new age data that were obtained by the LA-ICPMS recently set up at the Department of Geosciences, National Taiwan University. The analytical procedures for the SHRIMP method were same as those reported in Wen et al. (2008a). We describe below the LA-ICPMS techniques, using an Agilent 7500s quadrupole ICPMS and a New Wave UP213 laser ablation system housed at NTU. The operating conditions and data acquisition parameters are summarized in Table 1.

The laser ablation was performed with a helium carrier gas that can substantially reduce the deposition of ablated material onto the sample surface and greatly improve transport efficiency, and thus increase the signal intensities, as compared to “conventional” ablation

using argon as the carrier gas (Eggins et al., 1998; Günther and Heinrich, 1999; Jackson et al., 2004). During the experiments, about 1 min was spent for measuring gas blank and the results indicate sensitivities of less than 1000 counts per second (cps) for all measured isotopes. Calibration was performed using the GJ-1 zircon standard (provided by the Australian Research Council National Key Centre for Geochemical Evolution and Metallogeny of Continents, at Macquarie

**Table 1**  
LA-ICPMS operating conditions and data acquisition parameters.

Agilent 7500s ICPMS	
Forward power	1500 W
Gas flow rate:	
Plasma (Ar)	15 L/min
Auxiliary (Ar)	1 L/min
Carrier (He)	0.65–0.7 L/min
Make-up (Ar)	1.3–1.4 L/min
Oxide ion ( $\text{ThO}^+/\text{Th}^+$ )	≤0.3%
New Wave UP213 laser ablation system	
Wavelength	213 nm UV
Repetition rate	4 and 5 Hz
Spot size	30–50 $\mu\text{m}$
Energy	8–14 J/cm <sup>2</sup>
Data acquisition	
Data acquisition protocol	Time-resolved analysis (TRA)
Scanning mode	Peak hopping, 1 point per peak
Dwell time per isotope:	
$^{206}\text{Pb}$	15 ms
$^{207}\text{Pb}$	30 ms
$^{208}\text{Pb}$	30 ms
$^{232}\text{Th}$	10 ms
$^{238}\text{U}$	15 ms
Data acquisition time	130 s (60 s gas blank and 70 s ablation)

University, Sydney), well established for a precise  $^{207}\text{Pb}/^{206}\text{Pb}$  age and an intercept age using isotope-dilution thermal ionization mass spectrometry (ID-TIMS) at  $608.5 \pm 0.4$  Ma ( $2\sigma$ ) and  $608.5 \pm 1.5$  Ma ( $2\sigma$ ), respectively (Jackson et al., 2004). The Harvard reference zircon 91500 and Australian Mud Tank Carbonatite zircon (MT) were used as secondary standards for data quality control. All U-Th-Pb isotope ratios were calculated using the GLITTER 4.0 (GEMOC) software, and common lead was corrected using the common lead correction function proposed by Anderson (2002). The weighted mean U-Pb ages and concordia plots were carried out using Isoplot v. 3.0 (Ludwig, 2003).

Our LA-ICPMS results for the secondary zircon standards 91500 and MT, obtained during April 2006 and October 2007, are shown in the concordia diagrams (Fig. 3). The intercept,  $^{206}\text{Pb}/^{238}\text{U}$  and  $^{207}\text{Pb}/^{206}\text{Pb}$  ages of zircon 91500 are  $1061.8 \pm 2.1$  Ma ( $2\sigma$ ),  $1062.1 \pm 1.7$  Ma ( $2\sigma$ ) and  $1066.7 \pm 2.1$  Ma ( $2\sigma$ ), respectively (Fig. 3a–c), which are in perfect accordance with the consensus results reported by Wiedenbeck et al. (1995) using ID-TIMS method that gave  $^{207}\text{Pb}/^{206}\text{Pb}$  age at  $1065.4 \pm 0.6$  Ma ( $2\sigma$ ) and  $^{206}\text{Pb}/^{238}\text{U}$  age at  $1062.4 \pm 0.8$  Ma ( $2\sigma$ ). The intercept,

$^{206}\text{Pb}/^{238}\text{U}$  and  $^{207}\text{Pb}/^{206}\text{Pb}$  ages of zircon MT are  $736.8 \pm 5.2$  Ma ( $2\sigma$ ),  $734.0 \pm 2.4$  Ma ( $2\sigma$ ) and  $739.2 \pm 8.1$  Ma ( $2\sigma$ ), respectively (Fig. 3d–f), also well match the U-Pb concordia intercept age of  $732 \pm 5$  Ma reported by Black and Gulson (1978) using ID-TIMS method. Additionally, before starting routine U-Pb dating analysis, we established three “in-house” secondary zircons, which are igneous zircons separated from three Gangdese I-type granites, samples ST129A, ST143A and ST147A, whose  $^{206}\text{Pb}/^{238}\text{U}$  ages have been measured using the SHRIMP method that gave  $94.1 \pm 2.4$  Ma ( $2\sigma$ ),  $84.8 \pm 1.6$  Ma ( $2\sigma$ ) and  $50.6 \pm 0.7$  Ma ( $2\sigma$ ), respectively (Wen et al., 2008a). Our LA-ICPMS results of  $^{206}\text{Pb}/^{238}\text{U}$  ages of these three in-house zircon standards are  $96.4 \pm 0.6$  Ma ( $2\sigma$ ),  $86.2 \pm 0.6$  Ma ( $2\sigma$ ) and  $49.9 \pm 0.2$  Ma ( $2\sigma$ ), respectively (Fig. 4), which are all in good consistency with the SHRIMP results.

### 3.2. Zircon Lu–Hf isotopic measurements

In-situ Lu–Hf isotopic measurements were subsequently performed by the LA-MC-ICPMS method using a Thermo Finnigan Neptune

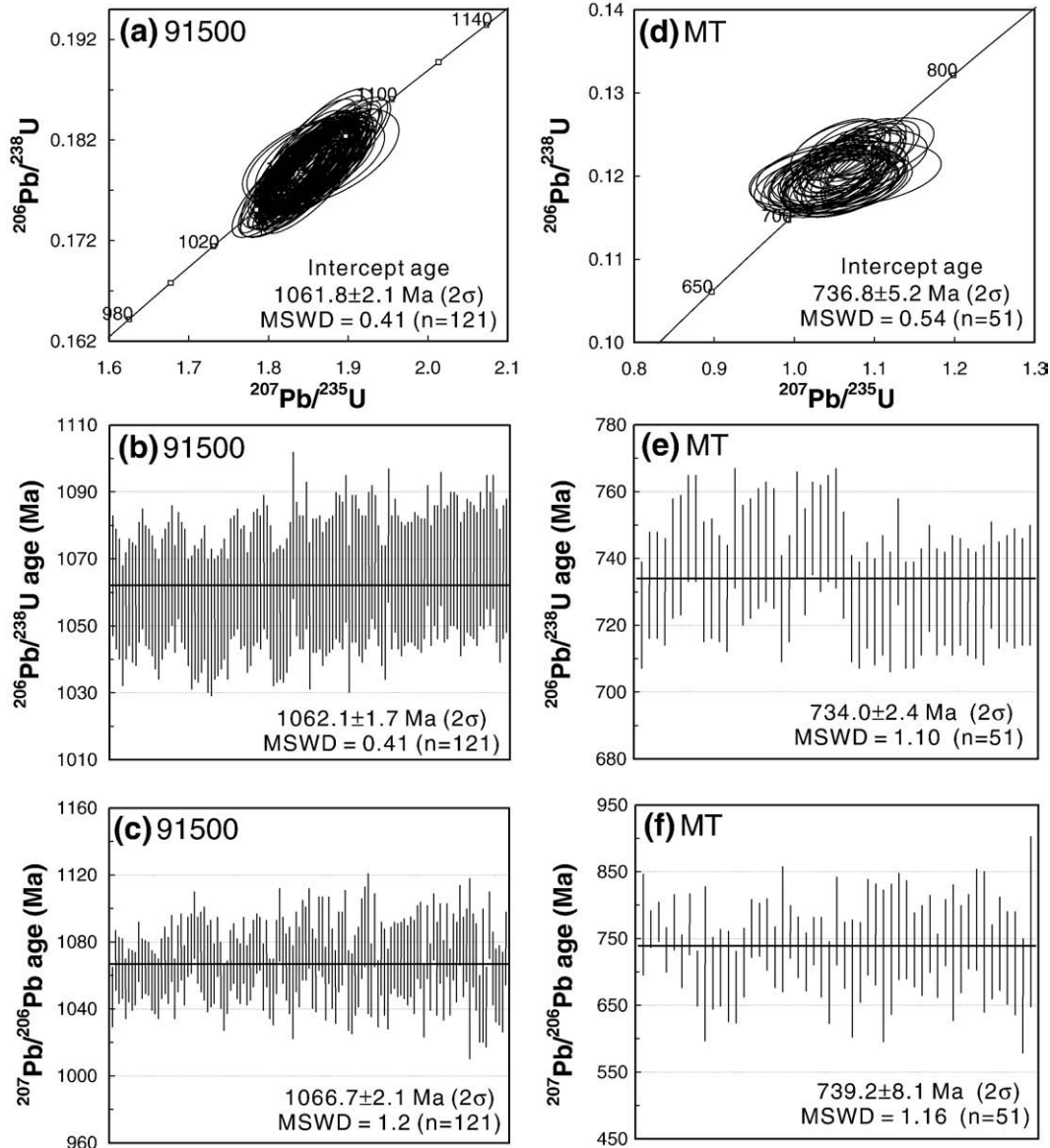


**Fig. 3.** U-Pb concordia diagrams of the zircon standards, (a) 91500 and (d) MT, analyzed by the LA-ICPMS at NTU. The long-term results and weighted averages of  $^{206}\text{Pb}/^{238}\text{U}$  and  $^{207}\text{Pb}/^{206}\text{Pb}$  ages are also shown.

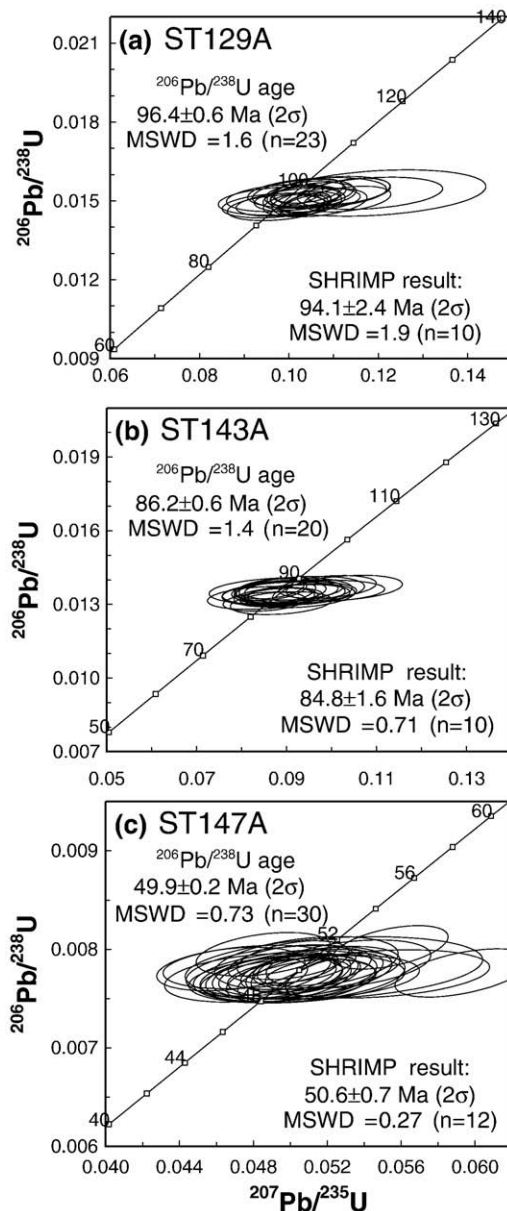


**Fig. 4.** U-Pb concordia diagrams of three in-house Gangdese zircon standards, (a) ST129A, (b) ST143A and (c) ST147A, analyzed by the LA-ICPMS at NTU. The SHRIMP results are also listed for comparison.

multicollectors-ICPMS and a Geolas CQ 193 nm laser ablation system housed at the Institute of Geology and Geophysics, Chinese Academy of Sciences, Beijing. Detailed descriptions for the analytical techniques can be found in Wu et al. (2006). The Lu-Hf isotopes were measured on the dated spots of individual zircons to minimize zoning effect but the laser ablation size is ~50–65  $\mu\text{m}$ , slightly larger than that of preexisting pits, sizing 30–50 mm, made by the U-Pb dating.

#### 4. Analytical results

##### 4.1. Zircon U-Pb ages

The zircons are mostly euhedral and reveal long to short prismatic forms (Fig. 2), with average crystal lengths of ~150–300  $\mu\text{m}$  and length-to-width ratios from 2:1 to 3:1. Most zircons are transparent, colorless to pale brown and show oscillatory zoning indicative of mag-

matic growth (Hoskin and Schaltegger, 2003). Zircons with rounded or oval shape and complex internal textures are rare. Thus, the interpretation of the zircon U-Pb isotopic data (see below) is simple and the obtained ages are interpreted as representing the crystallization time of the zircons dated and thus the emplacement timing of the host rocks.

The U-Pb age results are plotted in terms of concordia diagrams in Fig. 5 and summarized together with the coordinates of sample localities and rock types in Table 2. These include the  $^{206}\text{Pb}/^{238}\text{U}$  ages of 14 samples, based on a total of 215 individual zircon analyses, obtained by the LA-ICPMS method and those of 10 remaining samples, on 90 zircon grains, reported in Liang et al. (2008) using the SHRIMP method. Given that in zircon U-Pb isotopic analysis, precise age measurements using  $^{207}\text{Pb}/^{235}\text{U}$  and  $^{207}\text{Pb}/^{206}\text{Pb}$  ratios are feasible usually only for Precambrian zircons, due essentially to the fact that  $^{235}\text{U}$  comprises less than 1% of natural U and thus relatively little  $^{207}\text{Pb}$  can be produced in the Phanerozoic (cf. Ireland and Williams, 2003), the weighted mean of pooled  $^{206}\text{Pb}/^{238}\text{U}$  ages are taken to represent the crystallization ages of the dated samples. As shown in Fig. 5, all the mean ages are given at 95% confidence level, i.e.,  $2\sigma$  analytical uncertainties; coupled with their mean square of weighted deviates (MSWD). All U-Pb and Lu-Hf isotopic data are listed in Table 3.

In the Basu-Ranwu batholiths (Fig. 5a–h), eight samples dated indicate that the rocks were emplaced mainly in the Early Cretaceous (~130–115 Ma) except a granite (sample ET223A) that shows an apparently older emplacement age of ~198 Ma ( $197.7 \pm 1.5$  Ma; Fig. 5b) in the Jurassic. In the Bomi-Ranwu batholiths, there are ten samples being dated and eight of them exhibit Early Cretaceous U-Pb ages clustering around ~125–109 Ma. Two remaining samples, i.e., ET122E and ET014C (Table 2), show younger ages in the latest Cretaceous (~66 Ma) and Paleocene (~59 Ma), respectively. Six samples from the Chayu-Shama batholiths were dated and the results show two age populations (Table 2). These are a group of four granite samples from areas around the Chayu township (Fig. 1) that yielded Early Cretaceous ages (~133 Ma) and another group of two samples from areas close to Shama that show younger ages in the Paleocene (~60 Ma).

##### 4.2. Zircon Hf isotopic ratios

A total of 305 dated zircon grains from the 24 samples were analyzed for  $^{176}\text{Hf}/^{177}\text{Hf}$  isotopic ratios. The results are listed in Table 3 and  $\epsilon_{\text{Hf}}(T)$  data are plotted in Fig. 6, 8 and 9. The  $\epsilon_{\text{Hf}}(T)$  value, i.e., parts in  $10^4$  deviation of initial  $^{176}\text{Hf}/^{177}\text{Hf}$  isotopic ratios between the sample and the chondritic uniform reservoir, and  $T_{\text{DM}}^{\text{c}}$ , the zircon Hf isotope “crustal” model age based on a depleted-mantle source and an assumption that the protolith of the zircon’s host magma has the average continental crustal  $^{176}\text{Lu}/^{177}\text{Hf}$  ratio of 0.015, were calculated after Griffin et al. (2002) by utilizing the  $^{176}\text{Lu}-^{176}\text{Hf}$  decay constants adopted in Scherer et al. (2001). Our conclusions would not be significantly affected if the alternative decay constants proposed by more recent studies were used.

In the Basu-Ranwu batholiths (Fig. 6a–h), magmatic zircons exhibit exclusively negative  $\epsilon_{\text{Hf}}(T)$  values ranging from -1.9 to -18.1 except an “outlier” grain from sample ET234A that shows positive and the highest value of +0.5 (Fig. 6d). The zircon  $\epsilon_{\text{Hf}}(T)$  values are uniform within each sample, generally <4–ε unit variations, i.e., about the same as the external errors of the LA-MC-ICPMS analyses (Wu et al., 2006), except the Jurassic sample ET223A that displays a larger variation and the lowest  $\epsilon_{\text{Hf}}(T)$  value of -18.1 (Fig. 6b). In the Bomi-Ranwu batholiths (Fig. 6i–r), zircon  $\epsilon_{\text{Hf}}(T)$  values show a slightly wider range from +5.0 to -15.1. In addition, there are three samples, i.e., ET122E (Fig. 6k), ET120B (Fig. 6m) and ET117B (Fig. 6r), containing zircons that show positive  $\epsilon_{\text{Hf}}(T)$  values. Zircons from the Chayu-Shama batholiths, have exclusively negative  $\epsilon_{\text{Hf}}(T)$  values ranging from -4.4 to -20.0 (Fig. 6s–x). Occasionally,

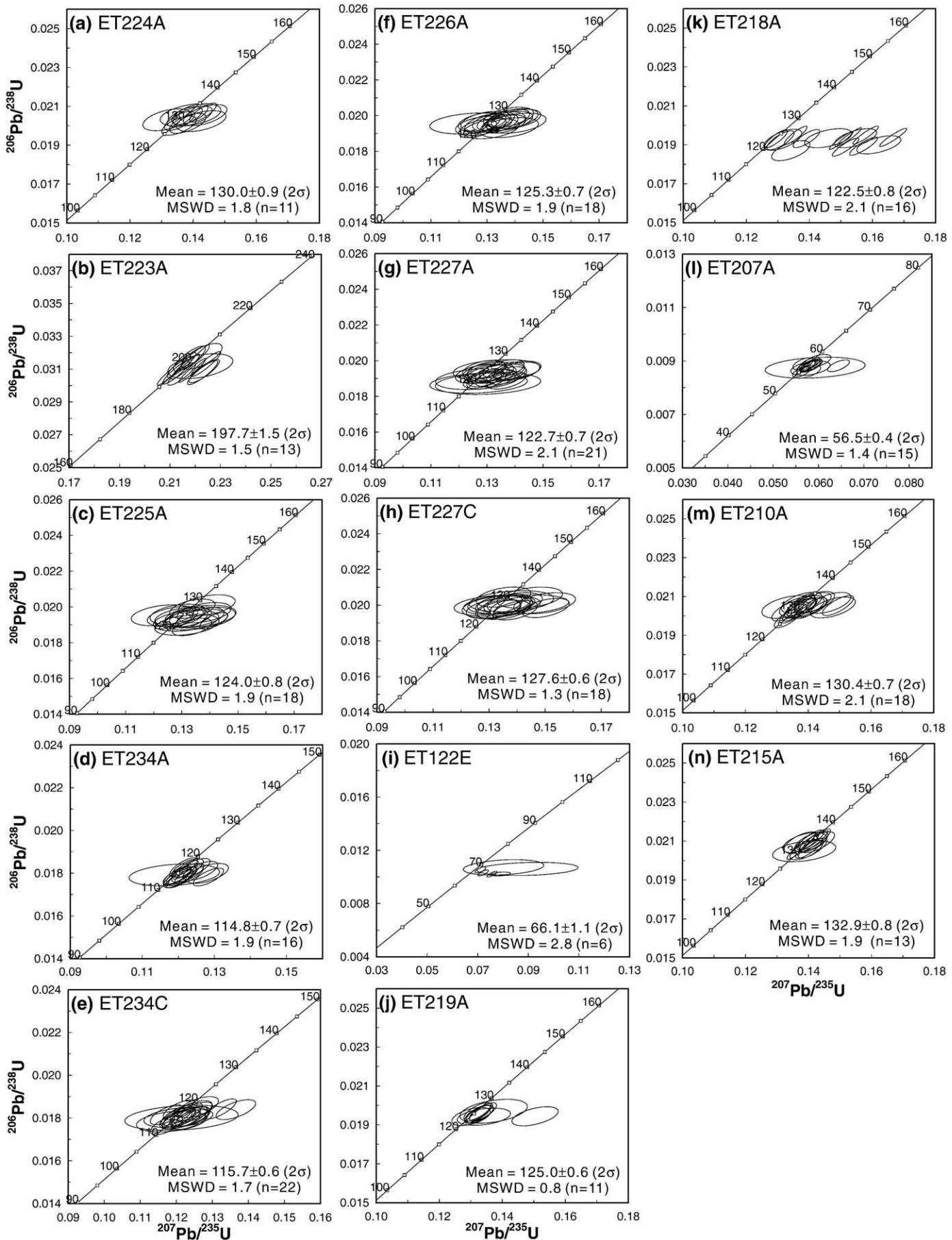


Fig. 5. Concordia diagrams of zircon U-Pb results of the eastern Himalayan batholiths. Note that the “mean” values of each sample are  $^{206}\text{Pb}/^{238}\text{U}$  ages in Ma.

**Table 2**

Summary of sample localities and zircon U–Pb ages of the eastern Himalayan batholiths, SE Tibet.

Sample	Longitude (°E)	Latitude (°N)	Elevation (m)	Rock type	Age (Ma)	$\pm 2\sigma$
<i>Basu–Ranwu batholiths</i>						
ET224A	96.6820	29.9001	3843	granite	130.0	0.9
ET223A	96.6869	29.8690	3870	granite	197.7	1.5
ET225A	96.6893	30.0058	3770	granodiorite	124.0	0.8
ET234A	96.7096	29.7649	4140	granite	114.8	0.7
ET234C	96.7096	29.7649	4140	enclave	115.7	0.6
ET226A	96.7252	30.0321	3668	granodiorite	125.3	0.7
ET227A	96.7868	30.0383	3462	granite	122.7	0.7
ET227C	96.7868	30.0383	3462	andesite	127.6	0.6
<i>Bomi–Ranwu batholiths</i>						
ET014C <sup>a</sup>	95.0700	30.1100	2176	granite	58.7	3.1
ET103B <sup>a</sup>	95.3845	29.9542	2636	granite (deformed)	118.6	2.0
ET122E	95.6971	29.7649	3745	granite	66.1	1.1
ET125B <sup>a</sup>	95.7163	29.7565	4072	granite (deformed)	125.1	1.5
ET120B <sup>a</sup>	96.0209	29.7417	3021	granite	109.0	1.1
ET104A <sup>a</sup>	96.6044	29.5075	3773	granite	114.8	1.7
ET219A	96.8515	29.3922	4201	granite	125.0	0.6
ET218A	96.8683	29.3855	4297	granite	122.5	0.8
ET106A <sup>a</sup>	96.8690	29.3855	4207	granite	122.5	1.5
ET117B <sup>a</sup>	97.1343	29.3213	3848	granite	116.9	1.8
<i>Chayu–Shama batholiths</i>						
ET113B <sup>a</sup>	97.0852	28.5616	1644	granite	59.1	3.2
ET207A	97.0865	28.5639	1701	granite	56.5	0.4
ET115E <sup>a</sup>	97.2496	28.5991	1896	granite (deformed)	133.1	1.3
ET210A	97.3661	28.6191	2166	granite (deformed)	130.4	0.7
ET215A	97.4034	28.9849	2884	granite	132.9	0.8
ET116A <sup>a</sup>	97.4698	28.6724	2319	granite	132.6	0.9

<sup>a</sup> SHRIMP results from Liang et al. (2008).

there are grains of inherited zircon detected in some samples, which are listed in Table 3 but not plotted in Fig. 6.

## 5. Discussion

### 5.1. Age distribution of the eastern Transhimalayan batholiths

Our results, combined with five zircon U–Pb ages reported by Booth et al. (2004) from the Bomi–Ranwu batholiths (Fig. 1) were plotted as an age histogram (Fig. 7a) that illustrates a major intrusive stage in the Early Cretaceous (~133–110 Ma) and a subordinate stage in the Paleocene (~66–57 Ma). This, however, does not imply the absence of igneous activity during Late Cretaceous time because the current dataset is far from being complete for making a conclusion on the age distribution. In fact, Liang et al. (2004) reported a detrital zircon study along the Yarlu–Tsangpo river system showing that zircons aged ~80–90 Ma are abundant in riverbank sediments recovered from the Parlung river flowing around the Bomi township. An inference is hence that magmatic rocks of Late Cretaceous ages, although not sampled so far from the surface exposures, are likely present in the region. Collectively, the age distribution pattern of the eastern Himalayan batholiths resembles in general to that of the northern plutonic belt (Fig. 7b) but differs from that of the Gangdese Batholith (Fig. 7c). The latter, emplaced in the southern margin of the central Lhasa terrane, shows a predominant stage of magmatism, or a magmatic “flare-up” event at ~50 Ma, in early Eocene time (Lee et al., 2007, this volume; Wen et al., 2008a).

In addition, this study identifies the first outcrop of Jurassic igneous rocks from the eastern Lhasa terrane, i.e., a granite body aged ~198 Ma in the Basu–Ranwu batholiths. Regardless of the scarcity, Jurassic magmatic records that are preserved/exposed sporadically in the central part (~84–94°E) of the Lhasa terrane have been reported in numerous recent studies using the zircon U–Pb method. These include: (1) Liang et al. (2004) that first reported the existence of abundant Jurassic inherited zircons (aged ~194–169 Ma) in a Cretaceous tuffaceous sandstone from the Gangdese belt; (2) Kapp et al. (2005b)

reporting abundant Jurassic inherited zircons (~204–181 Ma) in S-type granitoids from the Nyainqntanglha Range; (3) Chu et al. (2006) reporting Jurassic inherited zircons (~203–193 Ma) in two S-type granites from the northern plutonic belt, together with identifying an ~188 Ma granite body in the Gangdese Batholith; (4) Zhang et al. (2007a,b) reporting an ~178 Ma intrusion in the Gangdese Batholith and two Jurassic S-type granites (~205 and 202 Ma) in the southern margin of the northern plutonic belt; (5) Leier et al. (2007) reporting Jurassic and older detrital zircons (~180–220 Ma) in the Tekena Formation; (6) Zhu et al. (2008) reporting a Jurassic dacite (~174 Ma) in the Yeba Formation, and (7) Wu et al. (2009) reporting abundant Jurassic detrital zircons (~190–150 Ma) from the Late Cretaceous Xigaze fore-arc basin.

### 5.2. Zircon Hf isotopic characteristics of Transhimalayan batholiths

U–Pb and Hf isotope data of magmatic zircons from the eastern Himalayan batholiths are plotted in Fig. 8, from which several important features are observed: (1) they are dominated by negative  $\epsilon_{\text{Hf}}(T)$  values, (2) they show a wide spectrum of  $\epsilon_{\text{Hf}}(T)$  values ranging from +5 to -18, i.e., showing an ~23 units of  $\epsilon_{\text{Hf}}(T)$  variation, (3) zircons in two Cretaceous samples from the Bomi–Ranwu batholiths have the highest and positive  $\epsilon_{\text{Hf}}(T)$  values, in contrast to those from the Paleocene Chayu–Shama batholiths that show the lowest and negative  $\epsilon_{\text{Hf}}(T)$  values, and (4) overall speaking, the Hf isotope compositions of the Chayu–Shama batholiths appear to have become more radiogenic through time, a tendency that is unseen or absent in the Basu–Ranwu and Bomi–Ranwu batholiths.

Furthermore, also shown in Fig. 8, the overall distribution pattern of the eastern Himalayan batholiths emplaced in the eastern Lhasa terrane differs markedly from that of the Gangdese Batholith from the southern part of the central Lhasa terrane (Chu, 2006; Chu et al., 2006, in press; Zhang et al., 2007a; Wen et al., 2008a). Hence, in contrast to the Gangdese Batholith that requires involvement of a depleted or juvenile mantle as the major source component in the magma generation, affiliated closely with the Neo-Tethyan subduction zone

**Table 3**

U-Pb and Hf isotope data of igneous zircons from eastern Himalayan batholiths.

Spot	Th/U	$^{206}\text{Pb}/^{238}\text{U}$	$\pm 1\sigma$	$^{207}\text{Pb}/^{235}\text{U}$	$\pm 1\sigma$	Error corr.	$^{206}\text{Pb}/^{238}\text{U}$	age (Ma $\pm 1\sigma$ )	$^{176}\text{Hf}/^{177}\text{Hf} \pm 1\sigma$	$^{176}\text{Lu}/^{177}\text{Hf} \pm 1\sigma$	$\epsilon_{\text{Hf}}(T)$	$\pm 1\sigma$	$T_{\text{DM}}$	$T_{\text{DM}}$		
<i>ET224A wt. mean = 130.0 <math>\pm</math> 0.9 Ma (2<math>\sigma</math>)</i>																
ET224A-01	0.8130	0.0203	0.0002	0.1357	0.0020	0.6840	129.0	1.0	0.282443	6	0.001108	4	-8.91	0.20	1147	1752
ET224A-02	0.8772	0.0205	0.0002	0.1399	0.0025	0.5663	131.0	1.0	0.282402	6	0.000778	1	-10.29	0.23	1194	1841
ET224A-03	0.8475	0.0206	0.0002	0.1390	0.0023	0.6082	131.0	1.0	0.282407	7	0.001070	11	-10.13	0.26	1196	1830
ET224A-04	1.5152	0.0201	0.0002	0.1383	0.0024	0.6087	128.0	1.0	0.282404	7	0.001342	13	-10.34	0.25	1210	1841
ET224A-07	0.7194	0.0200	0.0002	0.1356	0.0022	0.6076	128.0	1.0	0.282401	6	0.000806	4	-10.40	0.22	1197	1845
ET224A-08	0.3861	0.0359	0.0004	0.2660	0.0032	0.8034	227.0	2.0	0.282378	6	0.002306	1	-9.30	0.22	1279	1849
ET224A-09	0.7813	0.0202	0.0002	0.1426	0.0032	0.4844	129.0	1.0	0.282444	10	0.000603	5	-8.82	0.36	1130	1746
ET224A-11	1.4925	0.0206	0.0002	0.1438	0.0028	0.5460	131.0	1.0	0.282423	7	0.000708	7	-9.53	0.26	1162	1792
ET224A-12	1.1236	0.0203	0.0002	0.1318	0.0031	0.4752	130.0	1.0	0.282413	7	0.000921	4	-9.93	0.25	1183	1817
ET224A-14	0.9434	0.0206	0.0002	0.1392	0.0039	0.4135	131.0	2.0	0.282399	8	0.000704	1	-10.38	0.29	1196	1846
ET224A-18	0.7246	0.0205	0.0002	0.1374	0.0023	0.6208	131.0	1.0	0.282387	7	0.000823	3	-10.80	0.26	1216	1873
ET224A-20	0.3717	0.0716	0.0007	0.5656	0.0062	0.8736	446.0	4.0	0.282402	8	0.001400	7	-3.67	0.29	1213	1659
ET224A-23	1.2658	0.0207	0.0002	0.1432	0.0017	0.8004	132.0	1.0	0.282435	8	0.001340	4	-9.13	0.27	1165	1768
ET224A-24	0.5618	0.1081	0.0011	1.0361	0.0113	0.8887	661.0	6.0	0.282424	8	0.000817	2	1.91	0.28	1165	1470
<i>ET223A wt. mean = 197.7 <math>\pm</math> 1.5 Ma (2<math>\sigma</math>)</i>																
ET223A-01	0.0332	0.0309	0.0003	0.2189	0.0022	0.9609	196.0	2.0	0.282427	5	0.001739	3	-8.13	0.19	1189	1752
ET223A-02	0.0476	0.0317	0.0003	0.2197	0.0024	0.8950	201.0	2.0	0.282466	9	0.002204	18	-6.69	0.30	1147	1664
ET223A-04	0.1590	0.0557	0.0006	0.4251	0.0048	0.8744	349.0	3.0	0.282177	8	0.001115	16	-13.62	0.28	1519	2214
ET223A-05	0.0078	0.0316	0.0003	0.2177	0.0026	0.8204	201.0	2.0	0.282141	10	0.001567	14	-18.11	0.35	1589	2385
ET223A-07	0.0394	0.0318	0.0003	0.2226	0.0033	0.6834	202.0	2.0	0.282468	13	0.001571	23	-6.51	0.45	1125	1654
ET223A-10	0.0527	0.0533	0.0006	0.4056	0.0054	0.8273	335.0	4.0	0.282488	10	0.002021	6	-3.13	0.35	1110	1540
ET223A-11	0.4630	0.0312	0.0003	0.2220	0.0053	0.4197	198.0	2.0	0.282430	8	0.002178	9	-8.05	0.28	1199	1748
ET223A-13	0.0388	0.0309	0.0003	0.2236	0.0025	0.8501	196.0	2.0	0.282537	13	0.002054	8	-4.27	0.45	1041	1508
ET223A-14	0.8772	0.0985	0.0010	0.8053	0.0097	0.8389	605.0	6.0	0.282285	9	0.000817	3	-4.23	0.32	1359	1815
ET223A-15	0.0286	0.0307	0.0003	0.2146	0.0023	0.8662	195.0	2.0	0.282348	7	0.001999	4	-10.96	0.25	1311	1931
ET223A-16	0.0580	0.0313	0.0003	0.2242	0.0024	0.9212	199.0	2.0	0.282413	9	0.001532	5	-8.53	0.31	1202	1780
ET223A-17	0.0273	0.0308	0.0003	0.2126	0.0023	0.9118	196.0	2.0	0.282509	10	0.003399	10	-5.43	0.34	1122	1581
ET223A-18	0.0228	0.0308	0.0003	0.2102	0.0022	0.9537	195.0	2.0	0.282405	7	0.002945	5	-9.09	0.26	1262	1812
ET223A-19	0.1818	0.0308	0.0003	0.2229	0.0025	0.8866	195.0	2.0	0.282283	11	0.001994	6	-13.29	0.40	1405	2077
ET223A-20	0.0192	0.0312	0.0003	0.2161	0.0023	0.9310	198.0	2.0	0.282498	12	0.002753	59	-5.71	0.43	1119	1600
ET223A-21	0.2725	0.0342	0.0003	0.2371	0.0025	0.9182	217.0	2.0	0.282484	9	0.002971	7	-5.86	0.31	1146	1624
ET223A-22	0.0500	0.0313	0.0003	0.2146	0.0024	0.9054	198.0	2.0	0.282462	10	0.002668	6	-6.97	0.34	1169	1680
<i>ET225A wt. mean = 124.0 <math>\pm</math> 0.8 Ma (2<math>\sigma</math>)</i>																
ET225A-02	0.8000	0.0189	0.0002	0.1336	0.0029	0.4948	121.0	1.0	0.282491	7	0.000755	1	-7.33	0.25	1069	1646
ET225A-03	0.8403	0.0193	0.0002	0.1349	0.0047	0.3607	123.0	2.0	0.282483	7	0.000750	4	-7.59	0.25	1081	1664
ET225A-05	0.8772	0.0195	0.0002	0.1231	0.0046	0.3326	125.0	2.0	0.282461	7	0.000562	1	-8.30	0.24	1105	1710
ET225A-07	0.9091	0.0194	0.0002	0.1305	0.0041	0.3751	124.0	1.0	0.282469	8	0.000793	3	-8.07	0.27	1101	1695
ET225A-08	1.0101	0.0190	0.0002	0.1318	0.0047	0.3557	121.0	2.0	0.282461	8	0.000648	1	-8.41	0.28	1108	1714
ET225A-09	0.6849	0.0193	0.0002	0.1287	0.0021	0.6244	123.0	1.0	0.282448	8	0.000985	3	-8.85	0.27	1136	1723
ET225A-10	0.9524	0.0192	0.0002	0.1414	0.0021	0.6785	123.0	1.0	0.282457	8	0.001199	1	-8.53	0.28	1130	1723
ET225A-11	0.7246	0.0193	0.0002	0.1335	0.0023	0.5906	123.0	1.0	0.282478	7	0.000999	7	-7.79	0.26	1095	1676
ET225A-12	0.9804	0.0194	0.0002	0.1354	0.0040	0.4034	124.0	1.0	0.282479	7	0.000717	4	-7.69	0.24	1085	1671
ET225A-13	0.9174	0.0199	0.0002	0.1338	0.0033	0.4468	127.0	1.0	0.282459	6	0.000786	1	-8.34	0.23	1114	1714
ET225A-14	0.9091	0.0196	0.0002	0.1285	0.0040	0.3745	125.0	1.0	0.282499	8	0.000767	1	-6.97	0.27	1058	1625
ET225A-15	0.7692	0.0201	0.0002	0.1390	0.0041	0.4039	128.0	2.0	0.282476	8	0.000570	3	-7.73	0.28	1085	1676
ET225A-16	1.0204	0.0197	0.0002	0.1380	0.0039	0.4113	126.0	1.0	0.282489	8	0.000782	3	-7.33	0.27	1073	1649
ET225A-17	0.9346	0.0195	0.0002	0.1277	0.0041	0.3699	124.0	1.0	0.282461	8	0.000675	1	-8.32	0.27	1108	1711
ET225A-18	0.9804	0.0192	0.0002	0.1315	0.0048	0.3456	123.0	2.0	0.282481	8	0.000606	2	-7.64	0.27	1079	1666
ET225A-19	0.8850	0.0195	0.0003	0.1367	0.0052	0.3393	124.0	2.0	0.282476	8	0.000621	1	-7.81	0.30	1086	1678
ET225A-20	0.7194	0.0194	0.0002	0.1300	0.0024	0.5980	124.0	1.0	0.282488	7	0.000907	6	-7.42	0.25	1078	1653
ET225A-21	1.2821	0.0194	0.0002	0.1387	0.0042	0.4068	124.0	2.0	0.282475	7	0.000992	1	-7.85	0.25	1098	1681
<i>ET234A wt. mean = 114.8 <math>\pm</math> 0.7 Ma (2<math>\sigma</math>)</i>																
ET234A-01	0.7092	0.0179	0.0002	0.1208	0.0017	0.6793	114.0	1.0	0.282622	7	0.001241	12	-2.89	0.26	897	1358
ET234A-02	0.7874	0.0179	0.0002	0.1198	0.0015	0.7387	114.0	1.0	0.282595	7	0.001631	3	-3.87	0.24	945	1420
ET234A-03	0.6944	0.0178	0.0002	0.1284	0.0017	0.7119	114.0	1.0	0.282619	7	0.001302	6	-3.00	0.23	903	1365
ET234A-04	0.7813	0.0181	0.0002	0.1261	0.0020	0.6362	116.0	1.0	0.282650	8	0.001181	8	-1.86	0.27	857	1294
ET234A-06	0.6757	0.0179	0.0002	0.1230	0.0016	0.7293	114.0	1.0	0.282622	7	0.001634	4	-2.94	0.26	908	1361
ET234A-07	0.6329	0.0182	0.0002	0.1226	0.0018	0.6796	117.0	1.0	0.282618	6	0.001197	5	-2.97	0.20	902	1365
ET234A-08	0.6667	0.0179	0.0002	0.1197	0.0016	0.7119	114.0</td									

**Table 3** (continued)

Spot	Th/U	$^{206}\text{Pb}/^{238}\text{U}$	$\pm 1\sigma$	$^{207}\text{Pb}/^{235}\text{U}$	$\pm 1\sigma$	Error corr.	$^{206}\text{Pb}/^{238}\text{U}$	age (Ma $\pm 1\sigma$ )	$^{176}\text{Hf}/^{177}\text{Hf} \pm 1\sigma$	$^{176}\text{Lu}/^{177}\text{Hf} \pm 1\sigma$	$\varepsilon_{\text{Hf}}(T)$	$\pm 1\sigma$	$T_{\text{DM}}$	$T_{\text{DM}}^{\text{C}}$		
<i>ET234C wt. mean = 115.7 <math>\pm 0.6</math> Ma (2<math>\sigma</math>)</i>																
ET234C-01	0.7634	0.0179	0.0002	0.1210	0.0023	0.5549	115.0	1.0	0.282561	9	0.001412	3	-5.05	0.33	989	1496
ET234C-02	0.7874	0.0184	0.0002	0.1247	0.0022	0.6004	117.0	1.0	0.282629	10	0.001932	6	-2.63	0.34	904	1344
ET234C-03	0.5917	0.0180	0.0002	0.1206	0.0039	0.3251	115.0	1.0	0.282575	8	0.001643	4	-4.58	0.30	975	1466
ET234C-05	0.6579	0.0184	0.0002	0.1211	0.0019	0.6485	117.0	1.0	0.282581	9	0.001613	7	-4.31	0.32	965	1451
ET234C-07	0.8000	0.0181	0.0002	0.1203	0.0018	0.7124	116.0	1.0	0.282577	8	0.001795	6	-4.49	0.28	976	1461
ET234C-08	0.6711	0.0178	0.0002	0.1186	0.0040	0.3358	114.0	1.0	0.282646	12	0.001924	9	-2.09	0.42	879	1307
ET234C-09	0.7576	0.0182	0.0002	0.1174	0.0019	0.6469	116.0	1.0	0.282586	8	0.001175	2	-4.11	0.28	947	1437
ET234C-10	0.8403	0.0181	0.0002	0.1204	0.0020	0.6435	115.0	1.0	0.282605	9	0.002756	18	-3.60	0.32	961	1404
ET234C-11	0.8850	0.0184	0.0002	0.1323	0.0018	0.7662	118.0	1.0	0.282540	8	0.001552	2	-5.75	0.27	1023	1543
ET234C-12	0.8547	0.0180	0.0002	0.1207	0.0019	0.6758	115.0	1.0	0.282542	8	0.001402	6	-5.73	0.28	1016	1539
ET234C-13	0.6369	0.0181	0.0002	0.1238	0.0023	0.5689	115.0	1.0	0.282591	9	0.001354	4	-3.98	0.30	944	1428
ET234C-14	0.6452	0.0180	0.0002	0.1214	0.0064	0.2521	115.0	2.0	0.282580	9	0.001147	5	-4.36	0.31	955	1453
ET234C-15	0.6410	0.0177	0.0002	0.1173	0.0018	0.6566	113.0	1.0	0.282606	8	0.001651	6	-3.50	0.29	930	1396
ET234C-16	0.7143	0.0185	0.0002	0.1260	0.0023	0.5895	118.0	1.0	0.282527	7	0.001697	5	-6.20	0.26	1044	1571
ET234C-17	0.7143	0.0183	0.0002	0.1250	0.0021	0.6276	117.0	1.0	0.282550	8	0.001741	3	-5.42	0.28	1013	1521
ET234C-18	0.7092	0.0183	0.0002	0.1227	0.0018	0.6982	117.0	1.0	0.282612	9	0.002247	13	-3.26	0.33	937	1384
ET234C-19	0.6711	0.0181	0.0002	0.1239	0.0022	0.5917	116.0	1.0	0.282553	12	0.001743	9	-5.34	0.42	1009	1515
ET234C-20	0.6757	0.0179	0.0002	0.1238	0.0021	0.6188	115.0	1.0	0.282573	8	0.001356	12	-4.61	0.28	970	1468
ET234C-22	0.6579	0.0181	0.0002	0.1216	0.0021	0.6151	115.0	1.0	0.282525	7	0.001209	6	-6.29	0.25	1034	1575
ET234C-23	0.6369	0.0184	0.0002	0.1365	0.0022	0.6297	117.0	1.0	0.282556	11	0.001255	6	-5.16	0.37	991	1504
ET234C-24	0.6849	0.0181	0.0002	0.1242	0.0018	0.7297	115.0	1.0	0.282566	9	0.001654	5	-4.87	0.31	987	1485
<i>ET226A wt. mean = 125.3 <math>\pm 0.7</math> Ma (2<math>\sigma</math>)</i>																
ET226A-01	0.9901	0.0199	0.0002	0.1377	0.0031	0.4778	127.0	1.0	0.282468	8	0.000825	3	-8.02	0.29	1103	1694
ET226A-02	0.9709	0.0197	0.0002	0.1378	0.0035	0.4445	126.0	1.0	0.282450	8	0.000753	2	-8.70	0.28	1127	1736
ET226A-03	1.0204	0.0196	0.0002	0.1405	0.0043	0.3829	125.0	1.0	0.282480	8	0.000694	1	-7.66	0.29	1083	1669
ET226A-04	0.9709	0.0198	0.0002	0.1403	0.0036	0.4315	127.0	1.0	0.282469	8	0.000687	1	-7.99	0.27	1098	1692
ET226A-05	1.0309	0.0197	0.0002	0.1296	0.0037	0.4150	126.0	1.0	0.282464	9	0.000900	1	-8.20	0.30	1111	1704
ET226A-06	0.9709	0.0196	0.0002	0.1346	0.0027	0.5431	125.0	1.0	0.282455	7	0.000914	1	-8.55	0.26	1124	1726
ET226A-07	1.1364	0.0197	0.0002	0.1342	0.0039	0.4068	126.0	1.0	0.282451	9	0.001045	14	-8.69	0.31	1134	1735
ET226A-08	0.8850	0.0196	0.0002	0.1283	0.0026	0.5343	125.0	1.0	0.282484	7	0.001038	2	-7.53	0.26	1087	1661
ET226A-09	1.0417	0.0199	0.0002	0.1377	0.0037	0.4357	127.0	1.0	0.282464	8	0.000927	7	-8.18	0.28	1112	1704
ET226A-10	0.9615	0.0198	0.0002	0.1391	0.0037	0.4324	127.0	1.0	0.282440	8	0.000898	3	-9.04	0.28	1145	1759
ET226A-12	1.0309	0.0194	0.0002	0.1278	0.0037	0.3922	124.0	1.0	0.282462	8	0.000709	0	-8.32	0.29	1109	1710
ET226A-13	0.9901	0.0197	0.0002	0.1331	0.0027	0.5223	126.0	1.0	0.282457	8	0.000839	2	-8.46	0.28	1120	1721
ET226A-14	0.8850	0.0196	0.0002	0.1283	0.0035	0.4128	125.0	1.0	0.282436	8	0.000528	2	-9.17	0.28	1139	1765
ET226A-15	1.0000	0.0195	0.0002	0.1362	0.0031	0.4678	125.0	1.0	0.282437	7	0.000696	2	-9.16	0.25	1142	1764
ET226A-16	0.9804	0.0196	0.0002	0.1243	0.0060	0.2545	125.0	2.0	0.282466	8	0.000642	4	-8.13	0.28	1101	1699
ET226A-17	0.9434	0.0193	0.0002	0.1316	0.0041	0.3868	123.0	1.0	0.282463	7	0.000681	0	-8.29	0.26	1106	1708
ET226A-18	0.9434	0.0193	0.0002	0.1378	0.0043	0.3814	123.0	1.0	0.282456	7	0.000616	2	-8.52	0.24	1113	1722
ET226A-22	1.0989	0.0193	0.0002	0.1267	0.0028	0.4999	123.0	1.0	0.282431	8	0.000970	4	-9.45	0.29	1160	1782
<i>ET227A wt. mean = 122.7 <math>\pm 0.7</math> Ma (2<math>\sigma</math>)</i>																
ET227A-01	0.6250	0.0189	0.0002	0.1283	0.0028	0.4890	121.0	1.0	0.282426	8	0.001011	7	-9.65	0.27	1167	1792
ET227A-02	0.6536	0.0192	0.0002	0.1316	0.0036	0.3977	123.0	1.0	0.282424	9	0.000732	1	-9.67	0.30	1162	1795
ET227A-03	0.6494	0.0192	0.0002	0.1370	0.0029	0.4863	122.0	1.0	0.282435	8	0.000852	0	-9.30	0.28	1150	1771
ET227A-04	0.6369	0.0195	0.0002	0.1299	0.0029	0.4681	124.0	1.0	0.282413	9	0.000823	1	-10.03	0.30	1179	1819
ET227A-05	1.2500	0.0193	0.0002	0.1284	0.0039	0.3722	123.0	1.0	0.282436	9	0.000965	1	-9.27	0.31	1152	1770
ET227A-06	0.9346	0.0195	0.0002	0.1335	0.0064	0.2587	124.0	2.0	0.282445	8	0.000807	1	-8.90	0.28	1134	1747
ET227A-07	0.6289	0.0195	0.0002	0.1359	0.0030	0.4836	125.0	1.0	0.282450	9	0.001024	3	-8.73	0.31	1134	1737
ET227A-08	0.8772	0.0193	0.0002	0.1349	0.0037	0.4010	123.0	1.0	0.282438	7	0.000798	1	-9.19	0.25	1145	1765
ET227A-09	1.0101	0.0195	0.0002	0.1406	0.0036	0.4261	124.0	1.0	0.282450	7	0.001018	1	-8.76	0.25	1134	1738
ET227A-10	0.6849	0.0190	0.0002	0.1296	0.0026	0.5218	122.0	1.0	0.282422	8	0.000773	1	-9.77	0.30	1166	1801
ET227A-11	0.6993	0.0193	0.0002	0.1297	0.0031	0.4542	123.0	1.0	0.282468	9	0.000889	2	-8.11	0.31	1104	1696
ET227A-13	1.3514	0.0189	0.0002	0.1369	0.0029	0.5083	121.0	1.0	0.282474	8	0.001507	16	-8.00	0.30	1115	1688
ET227A-14	0.6410	0.0190	0.0002	0.1266	0.0061	0.2618	121.0	2.0	0.282457	8	0.001089	7	-8.56	0.28	1126	1724
ET227A-15	1.1111	0.0194	0.0002	0.1304	0.0037	0.3995	124.0	1.0	0.282473	7	0.001317	8	-7.98	0.25	1111	1689
ET227A-16	0.7092	0.0194	0.0002	0.1406	0.0033	0.4557	124.0	1.0	0.282414	7	0.000999	3	-10.03	0.26	1184	1819
ET227A-17	1.0309	0.0190	0.0002	0.1331	0.0030	0.4681	121.0	1.0	0.282488	8	0.001063	4	-7.47	0.27	1082	1654
ET227A-18	0.7874	0.0187	0.0003	0.1304	0.0077	0.2270	120.0	2.0	0.282470	8	0.000831	1	-8.13	0.27	1101	1695
ET227A-19	0.9709	0.0194	0.0002	0.1354	0.0033	0.4496	124.0	1.0	0.282432	7	0.000908	2	-			

**Table 3** (continued)

Spot	Th/U	$^{206}\text{Pb}/^{238}\text{U}$	$\pm 1\sigma$	$^{207}\text{Pb}/^{235}\text{U}$	$\pm 1\sigma$	Error corr.	$^{206}\text{Pb}/^{238}\text{U}$ age (Ma $\pm 1\sigma$ )	$^{176}\text{Hf}/^{177}\text{Hf} \pm 1\sigma$	$^{176}\text{Lu}/^{177}\text{Hf} \pm 1\sigma$	$\varepsilon_{\text{Hf}}(T)$	$\pm 1\sigma$	$T_{\text{DM}}$	$T_{\text{DM}}^{\text{c}}$
<i>ET227C wt. mean = 127.6 ± 0.6 Ma (2σ)</i>													
ET227C-11	0.7463	0.0201	0.0002	0.1392	0.0040	0.3964	129.0	1.0	0.282513	8	0.000930	11	-6.42 0.28 1044 1593
ET227C-12	0.5435	0.0201	0.0002	0.1344	0.0049	0.2866	128.0	1.0	0.282503	7	0.000831	1	-6.77 0.25 1054 1615
ET227C-13	0.4566	0.0198	0.0002	0.1331	0.0033	0.4558	126.0	1.0	0.282513	7	0.000873	1	-6.48 0.24 1042 1596
ET227C-14	0.3846	0.0201	0.0002	0.1366	0.0034	0.4349	128.0	1.0	0.282507	7	0.000744	1	-6.61 0.23 1046 1605
ET227C-15	0.4785	0.0201	0.0002	0.1498	0.0045	0.3973	128.0	2.0	0.282560	8	0.001215	5	-4.80 0.30 985 1490
ET227C-16	0.6329	0.0200	0.0002	0.1421	0.0067	0.2341	128.0	1.0	0.282515	7	0.000660	1	-6.34 0.24 1033 1588
ET227C-17	0.6757	0.0204	0.0002	0.1445	0.0048	0.3569	130.0	2.0	0.282529	7	0.000892	1	-5.84 0.24 1021 1557
ET227C-18	0.4115	0.0197	0.0002	0.1393	0.0033	0.4769	126.0	1.0	0.282492	7	0.000789	1	-7.21 0.25 1069 1642
ET227C-19	0.4484	0.0199	0.0002	0.1379	0.0031	0.4855	127.0	1.0	0.282525	7	0.001021	2	-6.03 0.26 1029 1567
ET227C-20	0.6757	0.0198	0.0002	0.1316	0.0040	0.3822	126.0	1.0	0.282492	6	0.000746	1	-7.20 0.23 1067 1641
<i>ET014C<sup>a</sup> wt. mean = 58.7 ± 3.1 Ma (2σ)</i>													
ET014C-01.1	0.0263	0.0088	0.0002	0.1230	0.0197	0.1420	56.6	1.6	0.282469	9	0.000658	3	-9.52 0.32 1098 1736
ET014C-02.1	0.0385	0.0102	0.0002	0.1560	0.0374	0.0817	65.7	2.1	0.282502	7	0.000579	3	-8.13 0.26 1049 1655
ET014C-03.1	0.0213	0.0087	0.0003	0.1230	0.0221	0.1916	55.9	1.9	0.282457	10	0.000763	2	-9.95 0.35 1117 1763
ET014C-04.1	0.0266	0.0090	0.0002	0.0995	0.0067	0.3317	57.7	1.6	0.282526	9	0.000672	2	-7.46 0.33 1018 1606
ET014C-05.1	0.2123	0.0096	0.0002	0.0870	0.0084	0.2170	61.9	2.6	0.282504	9	0.001473	2	-8.18 0.33 1071 1655
ET014C-06.1	0.3306	0.0095	0.0002	0.0979	0.0082	0.2506	60.9	1.6	0.282476	14	0.001964	29	-9.21 0.50 1126 1719
<i>ET103B<sup>a</sup> wt. mean = 118.6 ± 2.0 Ma (2σ)</i>													
ET103B-02	1.8563	0.0188	0.0002	0.1307	0.0014	0.8245	120.0	1.0	0.282353	11	0.001098	14	-12.28 0.38 1273 1958
ET103B-03	1.1416	0.0184	0.0001	0.1341	0.0028	0.2864	117.4	0.7	0.282433	10	0.001363	13	-9.51 0.34 1168 1781
ET103B-04	2.1939	0.0185	0.0002	0.1324	0.0015	0.8065	118.0	1.0	0.282403	12	0.001304	26	-10.58 0.43 1210 1849
ET103B-05	1.8365	0.0192	0.0002	0.1348	0.0016	0.7906	122.0	1.0	0.282341	9	0.000677	2	-12.63 0.32 1276 1982
ET103B-06	2.2236	0.0187	0.0001	0.1309	0.0025	0.3343	119.1	0.8	0.282274	9	0.000676	6	-15.06 0.31 1368 2133
ET103B-08	2.2931	0.0182	0.0002	0.1226	0.0015	0.7500	116.0	1.0	0.282393	10	0.000658	2	-10.89 0.35 1202 1868
<i>ET122E wt. mean = 66.1 ± 1.1 Ma (2σ)</i>													
ET122E-01.1	0.4696	0.0107	0.0002	0.0802	0.0065	0.2716	68.7	1.5	0.282703	10	0.001021	2	-0.99 0.37 781 1207
ET122E-02.1	0.1336	0.0106	0.0002	0.0897	0.0082	0.2088	68.0	1.3	0.282872	9	0.000878	4	4.99 0.32 539 823
ET122E-L01	0.8537	0.0102	0.0001	0.0757	0.0008	0.8234	65.5	0.6	0.282694	14	0.002405	26	-1.44 0.48 824 1233
ET122E-L02	0.6055	0.0105	0.0001	0.0711	0.0009	0.6982	67.5	0.6	0.282714	20	0.005512	53	-0.84 0.71 870 1195
ET122E-L03	0.4666	0.0103	0.0001	0.0721	0.0008	0.7504	66.1	0.6	0.282797	15	0.002580	16	2.20 0.54 676 1000
ET122E-L08	1.0523	0.0102	0.0001	0.0791	0.0016	0.2997	65.5	0.4	0.282730	14	0.001559	11	-0.10 0.48 753 1148
<i>ET125B<sup>a</sup> wt. mean = 125.1 ± 1.5 Ma (2σ)</i>													
ET125B-01	0.5658	0.0191	0.0002	0.1292	0.0016	0.7568	122.0	1.0	0.282421	12	0.002058	25	-9.89 0.43 1208 1808
ET125B-03	1.0622	0.0196	0.0002	0.1370	0.0024	0.5729	125.0	1.0	0.282425	12	0.001923	26	-9.68 0.43 1198 1797
ET125B-04	0.8041	0.0199	0.0002	0.1353	0.0026	0.5285	127.0	1.0	0.282274	17	0.002001	7	-15.00 0.59 1418 2134
ET125B-05	1.3699	0.0195	0.0001	0.1414	0.0024	0.3276	124.8	0.7	0.282434	12	0.001723	18	-9.38 0.41 1179 1778
ET125B-06	1.5585	0.0196	0.0002	0.1334	0.0015	0.7945	125.0	1.0	0.282415	16	0.002565	19	-10.09 0.56 1234 1823
ET125B-07	0.8438	0.0199	0.0002	0.1358	0.0018	0.7334	127.0	1.0	0.282418	18	0.003074	30	-9.99 0.62 1247 1818
ET125B-10	0.7048	0.0196	0.0002	0.1354	0.0019	0.6804	125.0	1.0	0.282348	20	0.003001	16	-12.51 0.70 1348 1975
<i>ET120B<sup>a</sup> wt. mean = 109.0 ± 1.1 Ma (2σ)</i>													
ET120B-01.1	0.7767	0.0170	0.0004	0.1375	0.0072	0.4423	108.5	3.0	0.282754	12	0.002057	5	1.58 0.41 727 1069
ET120B-03.1	0.7318	0.0170	0.0003	0.1467	0.0091	0.3226	108.8	2.2	0.282732	13	0.001794	21	0.83 0.45 753 1117
ET120B-04.1	0.7565	0.0171	0.0004	0.1440	0.0187	0.1615	109.5	2.4	0.282333	13	0.002133	11	-13.28 0.46 1338 2013
ET120B-05.1	0.6089	0.0167	0.0003	0.1250	0.0058	0.4130	106.5	2.1	0.282818	13	0.003259	13	3.72 0.46 655 930
ET120B-06.1	0.6910	0.0174	0.0003	0.1490	0.0094	0.3175	111.1	1.73	0.282704	15	0.003740	27	-0.24 0.52 837 1187
ET120B-08.1	0.7776	0.0178	0.0004	0.1670	0.0110	0.3485	113.5	3.9	0.282656	27	0.002821	47	-1.81 0.96 886 1288
ET120B-09.1	0.5720	0.0172	0.0003	0.1209	0.0041	0.5588	110.0	2.2	0.282721	9	0.001465	9	0.50 0.33 762 1139
ET120B-10.1	0.8323	0.0166	0.0003	0.1270	0.0080	0.3016	106.3	2.1	0.282788	21	0.006029	39	2.46 0.76 760 1010
ET120B-13.1	1.0213	0.0181	0.0004	0.2320	0.0174	0.2800	115.4	2.8	0.282768	19	0.003128	31	2.14 0.66 727 1038
ET120B-14.1	0.6408	0.0169	0.0003	0.1460	0.0061	0.4762	108.2	2.7	0.282703	11	0.002286	23	-0.24 0.40 806 1185
ET120B-L01	1.3004	0.0168	0.0001	0.1112	0.0012	0.7746	107.1	0.9	0.282739	10	0.002652	24	1.00 0.36 760 1105
ET120B-L02	1.4196	0.0174	0.0002	0.1149	0.0013	0.7922	111.3	1.0	0.282710	10	0.002432	104	0.06 0.35 799 1168
ET120B-L03	0.7445	0.0167	0.0002	0.1112	0.0013	0.7498	106.9	1.0	0.282799	14	0.003116	80	3.08 0.49 680 972
ET120B-L04	1.5089	0.0172	0.0002	0.1158	0.0014	0.7427	109.9	1.0	0.282762	9	0.001928	34	1.90 0.33 713 1049
ET120B-L08	1.1912	0.0173	0.0002	0.1178	0.0014	0.7202	110.4	1.0	0.282767	17	0.002426	30	2.05 0.59 715 1040
<i>ET104A<sup>a</sup> wt. mean = 114.8 ± 1.7 Ma (2σ)</i>													
ET104A-01	0.7942	0.0180	0.0002	0.1205	0.0017	0.7166	115.0	1.0	0.282686	16	0.001818	15	-0.65 0.57 819 1216
ET104A-03	1.1615	0.0182	0.0002	0.1277	0.0019	0.6752	116.0	1.0	0.282641	12	0.002277	19	-2.28 0.42 896 1320
ET104A-05	1.1416	0.0178	0.0002	0.1257	0.0014	0.8443	114.0	1.0	0.282619	21	0.003388	38	-3.16 0.74 957 1375
ET104A-06	1.9159	0.0177	0.0001	0.1190	0.0018	0.4129	113.2	0.7	0.282707	17	0.002485	17	0.00 0.61 804 1173
ET104A-09	1.4493	0.0182	0.0001	0.1299	0.0026	0.3300	116.1	0.7	0.282553	19	0.002271	35	-5.36 0.67 1023 1516
<i>ET219A wt. mean = 125.0 ± 0.6 Ma (2σ)</i>													
ET219A-02	0.2262	0.0197	0.0002	0.1333	0.0015	0.8133	126.0	1.0	0.282607	10	0.002561	29	-3.27 0.34 952 1391
ET21													

**Table 3** (continued)

Spot	Th/U	$^{206}\text{Pb}/^{238}\text{U}$	$\pm 1\sigma$	$^{207}\text{Pb}/^{235}\text{U}$	$\pm 1\sigma$	Error corr.	$^{206}\text{Pb}/^{238}\text{U}$ age (Ma $\pm 1\sigma$ )	$^{176}\text{Hf}/^{177}\text{Hf} \pm 1\sigma$	$^{176}\text{Lu}/^{177}\text{Hf} \pm 1\sigma$	$\varepsilon_{\text{Hf}}(T)$	$\pm 1\sigma$	$T_{\text{DM}}$	$T_{\text{DM}}^{\text{C}}$
<i>ET219A wt. mean = 125.0 <math>\pm</math> 0.6 Ma (2<math>\sigma</math>)</i>													
ET219A-13	0.2457	0.0194	0.0002	0.1504	0.0030	0.5157	124.0	1.0	0.282475	6	0.002988	38	-8.02 0.21 1159 1690
ET219A-14	0.3610	0.0197	0.0002	0.1338	0.0018	0.7304	126.0	1.0	0.282449	5	0.003024	24	-8.92 0.19 1200 1749
ET219A-15	0.2591	0.0194	0.0002	0.1301	0.0025	0.5088	124.0	1.0	0.282489	5	0.002812	10	-7.51 0.18 1133 1658
ET219A-16	1.2048	0.0849	0.0008	0.6840	0.0085	0.7570	525.0	5.0	0.282139	7	0.000321	3	-10.93 0.26 1540 2176
ET219A-19	0.4902	0.0195	0.0002	0.1326	0.0019	0.6897	125.0	1.0	0.282423	7	0.001361	29	-9.71 0.25 1183 1799
<i>ET218A wt. mean = 122.5 <math>\pm</math> 0.8 Ma (2<math>\sigma</math>)</i>													
ET218A-02	0.2717	0.0214	0.0002	0.1460	0.0018	0.8175	137.0	1.0	0.282700	10	0.005449	77	-0.04 0.35 887 1193
ET218A-03	0.2625	0.0193	0.0002	0.1459	0.0031	0.4932	123.0	1.0	0.282524	8	0.004560	19	-6.45 0.28 1137 1590
ET218A-04	0.6024	0.0195	0.0002	0.1357	0.0015	0.8935	124.0	1.0	0.282692	11	0.007249	70	-0.71 0.38 951 1225
ET218A-05	0.6173	0.0211	0.0002	0.1665	0.0018	0.9151	135.0	1.0	0.282617	8	0.004759	32	-2.96 0.27 999 1377
ET218A-06	0.4785	0.0189	0.0002	0.1515	0.0017	0.8862	121.0	1.0	0.282528	15	0.003020	33	-6.22 0.53 1082 1574
ET218A-07	0.3040	0.0206	0.0002	0.1393	0.0017	0.8084	132.0	1.0	0.282465	6	0.003053	11	-8.21 0.21 1176 1709
ET218A-08	0.2532	0.0190	0.0002	0.1990	0.0020	0.9477	121.0	1.0	0.282644	13	0.008034	61	-2.51 0.45 1058 1337
ET218A-11	0.2252	0.0194	0.0002	0.1527	0.0016	0.9459	124.0	1.0	0.282514	7	0.003239	9	-6.68 0.24 1110 1606
ET218A-12	0.2427	0.0190	0.0002	0.1620	0.0029	0.5665	121.0	1.0	0.282499	10	0.004419	7	-7.36 0.34 1171 1646
ET218A-13	1.0526	0.0194	0.0002	0.1666	0.0018	0.9333	124.0	1.0	0.282621	7	0.004679	8	-3.02 0.26 990 1373
ET218A-15	0.1745	0.0187	0.0002	0.1341	0.0025	0.6047	119.0	1.0	0.282499	13	0.002709	31	-7.27 0.48 1116 1639
ET218A-17	0.1634	0.0192	0.0002	0.1501	0.0016	0.9507	123.0	1.0	0.282520	8	0.004973	14	-6.63 0.29 1158 1601
ET218A-18	0.1961	0.0193	0.0002	0.1315	0.0025	0.6083	123.0	1.0	0.282564	5	0.004397	16	-5.03 0.18 1070 1500
ET218A-19	0.7042	0.0193	0.0002	0.1391	0.0017	0.7951	123.0	1.0	0.282524	7	0.002961	6	-6.32 0.25 1086 1582
ET218A-20	0.7246	0.0189	0.0002	0.1572	0.0018	0.8717	121.0	1.0	0.282547	8	0.004676	21	-5.67 0.27 1105 1539
ET218A-21	0.3040	0.0192	0.0002	0.1308	0.0018	0.7687	123.0	1.0	0.282469	6	0.001635	4	-8.14 0.22 1126 1698
ET218A-22	0.5208	0.0195	0.0002	0.1579	0.0017	0.9266	124.0	1.0	0.282650	9	0.005832	52	-2.08 0.30 978 1313
ET218A-23	0.2740	0.0193	0.0002	0.1546	0.0027	0.5836	123.0	1.0	0.282472	7	0.004579	9	-8.27 0.23 1218 1705
ET218A-24	0.6250	0.0193	0.0002	0.1294	0.0015	0.8547	123.0	1.0	0.282476	8	0.001806	7	-7.93 0.27 1121 1684
<i>ET106A<sup>a</sup> wt. mean = 122.5 <math>\pm</math> 1.5 Ma (2<math>\sigma</math>)</i>													
ET106A-02	2.1542	0.0192	0.0002	0.1382	0.0015	0.8369	123.0	1.0	0.282394	15	0.003794	72	-10.99 0.53 1309 1878
ET106A-05	1.7174	0.0191	0.0002	0.1331	0.0012	0.9639	122.0	1.0	0.282375	19	0.005414	49	-11.81 0.68 1403 1927
ET106A-07	1.6876	0.0195	0.0002	0.1364	0.0015	0.8166	125.0	1.0	0.282487	18	0.005449	55	-7.79 0.65 1226 1676
ET106A-09	2.4123	0.0190	0.0001	0.1398	0.0017	0.4223	121.5	0.7	0.282350	20	0.006245	201	-12.78 0.71 1479 1987
ET106A-11	3.2561	0.0192	0.0001	0.1631	0.0018	0.4835	122.4	0.7	0.282436	14	0.003537	17	-9.48 0.49 1236 1782
<i>ET117B<sup>a</sup> wt. mean = 116.9 <math>\pm</math> 1.8 Ma (2<math>\sigma</math>)</i>													
ET117B-01.1	0.7684	0.0190	0.0004	0.1310	0.0068	0.3608	121.3	2.3	0.282567	7	0.000453	1	-4.64 0.24 956 1475
ET117B-02.1	0.4149	0.0178	0.0003	0.1180	0.0053	0.3392	113.6	1.7	0.282732	6	0.000427	2	1.05 0.22 725 1106
ET117B-03.1	0.6792	0.0181	0.0003	0.1282	0.0098	0.2238	115.9	2.0	0.282667	8	0.000564	3	-1.21 0.27 819 1252
ET117B-04.1	1.3521	0.0179	0.0004	0.1113	0.0061	0.4040	114.5	2.5	0.282748	9	0.000833	14	1.62 0.32 710 1071
ET117B-05.1	0.7137	0.0182	0.0006	0.1126	0.0255	0.1421	116.1	3.7	0.282717	7	0.000591	6	0.56 0.24 750 1140
ET117B-06.1	0.6798	0.0179	0.0003	0.1141	0.0093	0.2041	114.3	1.9	0.282686	7	0.000556	1	-0.56 0.24 792 1210
ET117B-07.1	0.9348	0.0185	0.0004	0.1078	0.0197	0.1135	118.2	2.4	0.282687	8	0.000518	1	-0.45 0.27 790 1206
ET117B-08.1	0.4084	0.0190	0.0003	0.1340	0.0052	0.3945	121.4	1.8	0.282486	12	0.000595	1	-7.49 0.41 1071 1656
ET117B-09.1	0.8598	0.0184	0.0004	0.1267	0.0093	0.3113	117.5	2.7	0.282707	9	0.000588	1	0.24 0.32 764 1161
ET117B-10.1	1.0428	0.0183	0.0003	0.1160	0.0159	0.1376	116.7	2.2	0.282676	8	0.000565	2	-0.87 0.27 806 1231
ET117B-11.1	0.9056	0.0185	0.0004	0.1006	0.0172	0.1106	118.4	2.2	0.282727	7	0.000553	1	0.96 0.26 735 1116
ET117B-12.1	0.9689	0.0181	0.0003	0.1054	0.0114	0.1690	115.5	2.1	0.282694	8	0.000816	6	-0.28 0.27 786 1193
<i>ET113B<sup>a</sup> wt. mean = 59.1 <math>\pm</math> 3.2 Ma (2<math>\sigma</math>)</i>													
ET113B-01.1	1.1869	0.0078	0.0006	-	-	-	50.0	4.0	0.282346	9	0.000491	2	-13.97 0.32 1262 2013
ET113B-03.1	1.0608	0.0085	0.0005	0.0460	0.0230	0.1060	54.7	2.9	0.282388	9	0.000716	2	-12.40 0.33 1211 1917
ET113B-04.1	0.1524	0.0091	0.0004	0.0330	0.0191	0.0828	58.5	2.8	0.282313	9	0.000525	2	-14.96 0.32 1308 2082
ET113B-05.1	1.5302	0.0086	0.0006	-	-	-	55.1	4.0	0.282379	9	0.000745	2	-12.71 0.33 1224 1937
ET113B-06.1	0.5007	0.0090	0.0004	0.0510	0.0138	0.1741	58.0	2.7	0.282396	8	0.000478	1	-12.05 0.30 1193 1897
ET113B-08.1	1.6361	0.0091	0.0005	0.0340	0.0231	0.0794	58.4	3.1	0.282375	9	0.000645	2	-12.80 0.30 1228 1945
ET113B-12.1	0.9068	0.0093	0.0004	0.0483	0.0092	0.2368	59.7	2.6	0.282406	8	0.000911	4	-11.66 0.28 1192 1874
ET113B-13.1	0.3566	0.0109	0.0005	0.0688	0.0043	0.7097	69.6	3.0	0.282397	9	0.000962	2	-11.77 0.32 1206 1888
ET113B-14.1	0.3155	0.0095	0.0006	-	-	-	60.8	3.7	0.282388	8	0.000518	2	-12.26 0.29 1205 1913
ET113B-15.1	0.3920	0.0086	0.0004	0.0476	0.0062	0.3769	55.1	2.7	0.282341	8	0.000900	2	-14.08 0.28 1283 2023
ET113B-17.1	1.4122	0.0091	0.0004	0.0550	0.0138	0.1960	58.2	2.9	0.282393	8	0.000651	2	-12.15 0.28 1202 1904
ET113B-18.1	0.1764	0.0105	0.0004	0.0665	0.0033	0.8600	67.1	2.9	0.282409	8	0.001033	5	-11.40 0.29 1192 1863
<i>ET207A wt. mean = 56.5 <math>\pm</math> 0.4 Ma (2<math>\sigma</math>)</i>													
ET207A-01	0.2212	0.0088	0.0001	0.0579	0.0010	0.5749	56.5	0.6	0.282367	8	0.001500	9	-13.14 0.28 1267 1965
ET207A-02	0.0986	0.0246	0.0002	0.1700	0.0019	0.8600	157.0	2.0	0.282368	7	0.000955	3	-10.93 0.24 1246 1900
ET207A-03	0.1923	0.0088	0.0001	0.0576	0.0008	0.7736	56.6	0.6	0.282172	8	0.001127	2	-20.03 0.27 1528 2400
ET207A-04	0.0567	0.0086	0.0001	0.0567	0.0007	0.7426	55.2	0.5	0.282275	8	0.001642	1	-16.42 0.27 1402 2171
ET207A-07	0.4082	0.0088	0.0001	0.0572	0.0009	0.6894	56.4	0.6	0.282408	10	0.001325	5	-11.68

**Table 3 (continued)**

Spot	Th/U	$^{206}\text{Pb}/^{238}\text{U}$	$\pm 1\sigma$	$^{207}\text{Pb}/^{235}\text{U}$	$\pm 1\sigma$	Error corr.	$^{206}\text{Pb}/^{238}\text{U}$ age (Ma $\pm 1\sigma$ )	$^{176}\text{Hf}/^{177}\text{Hf} \pm 1\sigma$	$^{176}\text{Lu}/^{177}\text{Hf} \pm 1\sigma$	$\varepsilon_{\text{Hf}}(T)$	$\pm 1\sigma$	$T_{\text{DM}}$	$T_{\text{DM}}^{\text{c}}$
<i>ET207A wt. mean = 56.5 ± 0.4 Ma (2σ)</i>													
ET207A-15	0.6452	0.0186	0.0002	0.1254	0.0021	0.6100	119.0	1.0	0.282669	7	0.000665	2	-1.08 0.24 818 1247
ET207A-16	0.1269	0.0087	0.0001	0.0582	0.0018	0.4145	56.0	0.7	0.282341	6	0.001447	18	-14.05 0.23 1301 2022
ET207A-17	0.2915	0.0088	0.0001	0.0583	0.0009	0.6929	56.5	0.6	0.282390	8	0.001093	3	-12.30 0.27 1220 1912
ET207A-18	0.2882	0.0089	0.0001	0.0581	0.0009	0.6244	57.2	0.6	0.282395	6	0.001296	7	-12.11 0.20 1220 1900
ET207A-20	0.4049	0.0088	0.0002	0.0593	0.0045	0.2408	56.0	1.0	0.282393	7	0.001161	5	-12.23 0.24 1219 1907
ET207A-21	0.3390	0.0088	0.0001	0.0586	0.0009	0.6483	56.7	0.6	0.282371	7	0.001484	4	-12.98 0.23 1260 1955
ET207A-22	0.0927	0.0088	0.0001	0.0578	0.0008	0.7368	56.7	0.6	0.282332	6	0.001761	6	-14.38 0.21 1325 2043
ET207A-23	0.1040	0.0089	0.0001	0.0585	0.0010	0.6188	56.9	0.6	0.282323	9	0.000989	1	-14.67 0.31 1311 2062
ET207A-24	0.1403	0.0090	0.0001	0.0597	0.0012	0.5441	57.8	0.6	0.282315	6	0.000622	2	-14.93 0.20 1310 2079
<i>ET115E<sup>a</sup> wt. mean = 133.1 ± 1.3 Ma (2σ)</i>													
ET115E-01.1	0.7346	0.0204	0.0002	0.1497	0.0100	0.1834	130.1	1.6	0.282517	7	0.000839	1	-6.23 0.24 1035 1583
ET115E-02.1	0.7729	0.0206	0.0003	0.1270	0.0133	0.1198	131.6	1.6	0.282512	6	0.000839	5	-6.40 0.19 1043 1594
ET115E-03.1	0.8242	0.0212	0.0004	0.1716	0.0335	0.1040	134.9	2.7	0.282513	7	0.000722	1	-6.27 0.25 1038 1589
ET115E-04.1	1.0117	0.0214	0.0002	0.1435	0.0077	0.1799	136.6	1.3	0.282521	7	0.000946	11	-5.97 0.23 1033 1571
ET115E-05.1	1.7911	0.0207	0.0002	0.1364	0.0049	0.2301	132.4	1.1	0.282501	6	0.000741	9	-6.73 0.21 1054 1616
ET115E-06.1	0.9383	0.0206	0.0003	0.1574	0.0114	0.1894	131.2	1.8	0.282455	5	0.000763	4	-8.40 0.19 1119 1721
ET115E-07.1	0.8043	0.0207	0.0002	0.1424	0.0068	0.2348	132.0	1.5	0.282529	6	0.000811	10	-5.77 0.22 1018 1555
ET115E-08.1	0.6468	0.0205	0.0003	0.1308	0.0170	0.1141	130.6	1.9	0.282435	8	0.001031	5	-9.15 0.28 1156 1768
ET115E-09.1	0.8116	0.0212	0.0003	0.1458	0.0099	0.2180	135.2	2.0	0.282487	6	0.000649	1	-7.19 0.22 1072 1647
ET115E-10.1	0.7396	0.0209	0.0002	0.1402	0.0060	0.2244	133.6	1.3	0.282545	8	0.000779	3	-5.16 0.27 994 1517
ET115E-11.1	0.7372	0.0212	0.0002	0.1451	0.0131	0.1261	135.3	1.5	0.282509	7	0.000704	2	-6.41 0.23 1043 1598
ET115E-12.1	0.7807	0.0206	0.0005	0.0845	0.0624	0.0358	131.7	3.4	0.282491	6	0.000622	7	-7.09 0.21 1065 1638
<i>ET210A wt. mean = 130.4 ± 0.7 Ma (2σ)</i>													
ET210A-01	0.4032	0.0205	0.0002	0.1495	0.0020	0.7532	131.0	1.0	0.282450	8	0.001282	9	-8.63 0.27 1142 1735
ET210A-03	0.6944	0.0204	0.0002	0.1375	0.0021	0.6843	130.0	1.0	0.282491	8	0.001283	2	-7.20 0.29 1084 1644
ET210A-04	0.4762	0.0199	0.0002	0.1335	0.0018	0.7631	127.0	1.0	0.282572	7	0.001289	1	-4.39 0.25 969 1463
ET210A-05	0.5650	0.0203	0.0002	0.1335	0.0021	0.6686	129.0	1.0	0.282437	7	0.000761	0	-9.09 0.24 1145 1763
ET210A-06	0.4444	0.0202	0.0002	0.1360	0.0017	0.7957	129.0	1.0	0.282502	7	0.001503	1	-6.84 0.24 1075 1620
ET210A-09	0.6135	0.0204	0.0002	0.1404	0.0024	0.6136	130.0	1.0	0.282464	7	0.000887	2	-8.11 0.24 1110 1702
ET210A-11	0.4831	0.0204	0.0002	0.1405	0.0019	0.7618	130.0	1.0	0.282469	7	0.001112	1	-7.95 0.24 1110 1691
ET210A-13	0.5587	0.0205	0.0002	0.1376	0.0019	0.7372	131.0	1.0	0.282549	7	0.001044	1	-5.10 0.24 996 1511
ET210A-14	0.3367	0.0201	0.0002	0.1352	0.0017	0.7723	128.0	1.0	0.282442	7	0.001302	2	-8.97 0.23 1154 1755
ET210A-15	0.4831	0.0207	0.0002	0.1379	0.0018	0.7965	132.0	1.0	0.282355	6	0.001308	8	-11.98 0.21 1278 1948
ET210A-16	0.5291	0.0204	0.0002	0.1382	0.0019	0.7404	130.0	1.0	0.282489	6	0.001096	1	-7.25 0.21 1082 1647
ET210A-17	0.6711	0.0207	0.0002	0.1379	0.0026	0.5558	132.0	1.0	0.282463	8	0.000809	1	-8.09 0.27 1109 1702
ET210A-18	0.6173	0.0205	0.0002	0.1338	0.0035	0.4496	131.0	2.0	0.282422	7	0.000856	1	-9.58 0.24 1168 1795
ET210A-19	0.6897	0.0207	0.0002	0.1420	0.0026	0.5754	132.0	1.0	0.282502	7	0.000875	2	-6.72 0.24 1057 1615
ET210A-20	0.6667	0.0204	0.0002	0.1479	0.0029	0.5434	130.0	1.0	0.282441	6	0.000760	0	-8.91 0.22 1139 1752
ET210A-21	0.6711	0.0207	0.0002	0.1468	0.0028	0.5662	132.0	1.0	0.282471	7	0.000864	2	-7.84 0.26 1101 1686
ET210A-22	0.6061	0.0205	0.0002	0.1384	0.0031	0.5059	131.0	1.0	0.282467	7	0.000760	2	-7.99 0.24 1103 1695
ET210A-23	0.5917	0.0207	0.0002	0.1414	0.0024	0.6248	132.0	1.0	0.282450	7	0.000848	1	-8.56 0.24 1129 1732
<i>ET215A wt. mean = 132.9 ± 0.8 Ma (2σ)</i>													
ET215A-02	0.3937	0.0210	0.0002	0.1423	0.0016	0.9053	134.0	1.0	0.282493	10	0.003679	14	-7.26 0.37 1155 1650
ET215A-03	0.4950	0.0210	0.0002	0.1409	0.0022	0.6534	134.0	1.0	0.282375	8	0.001652	3	-11.25 0.28 1261 1903
ET215A-07	0.4566	0.0209	0.0002	0.1386	0.0016	0.8992	133.0	1.0	0.282422	7	0.003581	6	-9.76 0.25 1258 1807
ET215A-08	0.3953	0.0206	0.0002	0.1367	0.0015	0.9113	131.0	1.0	0.282399	8	0.003506	3	-10.62 0.28 1291 1860
ET215A-12	0.4902	0.0209	0.0002	0.1428	0.0023	0.6636	134.0	1.0	0.282365	7	0.001619	3	-11.60 0.24 1274 1925
ET215A-14	0.4484	0.0206	0.0002	0.1402	0.0017	0.8249	132.0	1.0	0.282476	8	0.004158	48	-7.94 0.28 1197 1691
ET215A-15	0.5076	0.0209	0.0002	0.1377	0.0022	0.6518	134.0	1.0	0.282380	7	0.001833	1	-11.09 0.25 1260 1893
ET215A-16	0.5435	0.0206	0.0002	0.1394	0.0021	0.6686	131.0	1.0	0.282414	7	0.001566	10	-9.92 0.24 1202 1817
ET215A-17	0.5000	0.0209	0.0002	0.1388	0.0028	0.5145	133.0	1.0	0.282331	7	0.001665	5	-12.82 0.24 1323 2002
ET215A-18	0.4630	0.0205	0.0002	0.1386	0.0041	0.3632	131.0	1.0	0.282386	7	0.001847	9	-10.93 0.26 1251 1881
ET215A-19	0.4808	0.0206	0.0002	0.1413	0.0019	0.7648	132.0	1.0	0.282372	8	0.002514	10	-11.47 0.27 1295 1915
ET215A-21	0.4065	0.0211	0.0002	0.1427	0.0017	0.8208	135.0	1.0	0.282400	6	0.003099	4	-10.47 0.21 1274 1853
ET215A-22	0.4608	0.0211	0.0002	0.1407	0.0017	0.8111	134.0	1.0	0.282378	10	0.002563	12	-11.21 0.36 1287 1900
<i>ET116A<sup>a</sup> wt. mean = 132.6 ± 0.9 Ma (2σ)</i>													
ET116A-01.1	0.4485	0.0206	0.0001	0.1298	0.0040	0.1690	131.4	0.7	0.282415	5	0.001404	1	-9.85 0.18 1195 1813
ET116A-02.1	0.3603	0.0208	0.0002	0.1395	0.0066	0.1858	132.8	1.2	0.282412	6	0.001069	10	-9.93 0.20 1190 1819
ET116A-03.1	0.5438	0.0210	0.0001	0.1412	0.0047	0.1612	134.2	0.7	0.282374	6	0.001031	3	-11.23 0.21 1241 1902
ET116A-05.1	0.8638	0.0209	0.0002	0.1427	0.0068	0.1924	133.2	1.2	0.282493	6	0.001054	21	-7.05 0.22 1075 1637
ET116A-06.1	0.4203	0.0210	0.0002	0.1379	0.0036	0.3660	134.0	1.3	0.282417	5	0.001083	5	-9.71 0.19 1182 1806
ET116A-08.1	1.3504	0.0207	0.0002	0.1321	0.0095	0.1597	132.1	1.5	0.282498	6	0.001045	6	-6.89 0.21 1068 1625
ET116A-09.1	0.7021	0.0211	0.0001	0.1403	0.0060	0.1593	134.3	0.9	0.282395	5	0.001474	22	-10.51 0.17 1226 1857
ET116A-													

processes (Chu et al., 2006, *in press*), the granitoid genesis in the eastern Himalayan batholiths involves a significant contribution by old continental crust. Given the similarities in zircon U-Pb and Hf isotope systematics (Fig. 8), the petrogenesis may resemble to that of S-type granites in the northern plutonic belt (Chu et al., 2006), resulting largely from anatexis or remelting of the Proterozoic crust (see below).

### 5.3. Implications for the petrogenesis and crustal evolution

Zircons can effectively preserve the initial Hf isotope ratios of the host magmas so their Hf isotope compositions may be utilized in exactly the same way that whole-rock Nd isotopes have been utilized as a powerful geochemical tracer for petrogenesis. The Hf “crustal” model ages, or  $T_{\text{DM}}^{\text{C}}$ , of zircons, can therefore give reasonable estimates of the timing since which their host magmas were derived from the presumed depleted-mantle source (cf. Griffin et al., 2002). For example, granites that formed by partial melting of old crustal rocks would show zircon Hf crustal model ages much older than their crystallization ages. By contrast, granites that originated from a juvenile mantle source have “young” model ages that are slightly older than or even close to their crystallization ages. More specifically, zircons from the Gangdese Batholith that exhibit juvenile mantle Hf isotope characteristics yield Phanerozoic  $T_{\text{DM}}^{\text{C}}$  ages peaked at ~300–400 Ma (Fig. 9e). However, zircons from the S-type granites in the northern plutonic belt display obviously older  $T_{\text{DM}}^{\text{C}}$  ages from ca. 1.0 to 2.3 Ga, clustering at ~1.7 Ga (Fig. 9e), which led Chu et al. (2006) to conclude that a major stage of the continental crust growth occurred during late Paleoproterozoic and early Mesoproterozoic time in the northern Lhasa terrane. This Proterozoic crust that remelted in the Jurassic–Early Cretaceous was the principal source region of the S-type granites formed (Chu et al., 2006).

In the eastern Lhasa terrane, all zircons analyzed by this study have old  $T_{\text{DM}}^{\text{C}}$  ages between 0.8 and 2.4 Ga that are also peaked at ~1.7 Ga (Fig. 9a–d), which therefore can be interpreted by the same scenarios, i.e., a significant continental crustal formation in the Proterozoic and remelting of this crust during the early Jurassic. This zircon Hf isotope evidence for a major episode of Proterozoic crustal growth in the eastern Lhasa terrane is in good consistency with whole-rock Nd isotopic constraints from the eastern Himalayan batholiths (Lin, 2007; Lin et al., 2007), which show low  $\varepsilon_{\text{Nd}}(T)$  isotopic values between –2.6 and –12.6 thus yielding the depleted-mantle model ages ( $T_{\text{DM}}$ ) between ~0.9 and 2.5 Ga. In the Bomi–Ranwu batholiths, the three samples (i.e., ET122A ≈ 66 Ma; ET120A ≈ 109 Ma; and ET117A ≈ 117 Ma; Figs. 5 and 6) that show positive zircon  $\varepsilon_{\text{Hf}}(T)$  values are marked by apparently younger  $T_{\text{DM}}^{\text{C}}$  ages (Fig. 9b and c), coupled with higher whole-rock  $\varepsilon_{\text{Nd}}(T)$  values from –2.6 to –6.5 (Lin, 2007; Lin et al., 2007), suggesting the juvenile mantle source region to have played a role in the magma genesis. By contrast, most of the eastern Himalayan batholiths exhibit zircon  $\varepsilon_{\text{Hf}}(T)$  values < –10 and whole-rock  $\varepsilon_{\text{Nd}}(T)$  values of –10 to –12.6, which yield zircon  $T_{\text{DM}}^{\text{C}}$  and whole-rock  $T_{\text{DM}}$

ages both between ~1.5 and 2.5 Ga, suggesting a predominantly, or even exclusively, old continental crust source that remelted to produce the granitoids.

### 5.4. Precollisional tectono-magmatic evolution in southern Tibet

We synthesize in Fig. 10 all zircon U-Pb age data of igneous rocks in the Lhasa terrane to examine the precollisional magmatic evolution in southern Tibet. These include three magma suites, namely, the Gangdese Batholith and associated Linzizong volcanic successions, the northern plutonic belt, and the eastern Himalayan batholiths. “Postcollisional” igneous rocks, e.g., Late Oligocene to Middle Miocene adakites and ultrapotassic rocks (Chung et al., 2003, 2005), are excluded from the synthesis. Note that the three shaded east–west-trending regions in Fig. 10 were adopted from Leier et al. (2007) that highlighted general magmatic trends in the Tibetan plateau, which, from north to south, denote the Paleozoic, Triassic and Late Cretaceous igneous activities corresponding broadly to the long-lived, northward terrane suturing/accretion and associated subduction processes in the entire region. Despite a major magmatic period of ~150–100 Ma was postulated by Leier et al. (2007) based essentially on age data from the northern Lhasa terrane (Fig. 10), we here address the importance of Late Cretaceous to Paleogene magmatism that caused the principal components of the Gangdese and Linzizong rocks now exposed in the southern margin of the Lhasa terrane (Chung et al., 2005; Mo et al., 2005, 2007; Lee et al., 2007, this volume; Wen et al., 2008a).

Most recently, Wu et al. (2009) conducted a zircon U-Pb and Hf isotopic study in the Late Cretaceous Xigaze fore-arc basin, located immediately south of the Gangdese Batholith and north of the Yarlung-Tsangpo suture (Fig. 10). The results suggest not only that the Gangdese Batholith was the predominant source provenance, but also that during the fore-arc deposition the Gangdese arc exposure was dominated by igneous rocks formed ~130–80 Ma (peaked at ~110 Ma), associated in a smaller amount with those formed ~190–150 Ma, thereby recording two important stages of the arc magmatism that are only sporadically observed in the modern outcrops as a result of significant erosion related to the mountain uplift during Cenozoic time. The results, furthermore, support the argument by Chu et al. (2006) for the existence of a long-lasting Neo-Tethyan subduction system that began since the early Jurassic, soon after the Lhasa terrane rifted from Gondwanaland, and lasted until beginning of the India-Asia collision that closed the Neo-Tethys ocean.

As stated in preceding sections, the ages, zircon Hf isotopes and whole-rock geochemical characteristics of the eastern Himalayan batholiths are all comparable to those of the northern plutonic belt but different markedly from those of the Gangdese Batholith. This leads us to conclude that the former two suites should be correlated each other in the petrogenesis, and the eastward equivalent of the Gangdese Batholith, if existing, may be exposed in the areas immediately north of the suture (Fig. 10), where, unfortunately, is around the Chinese–

#### Notes to Table 3

$\lambda_{\text{Lu}-\text{Hf}} = 1.86 \times 10^{-11} \text{ year}^{-1}$ .
$\varepsilon_{\text{Hf}}(T) = [(\text{176Hf}/\text{177Hf})_{\text{Sample}}/(\text{176Hf}/\text{177Hf})_{\text{CHUR}} - 1] \times 10^4$ .
$\varepsilon_{\text{Hf}}(T) = \{[(\text{176Hf}/\text{177Hf})_{\text{Sample}}^0 - (\text{176Lu}/\text{177Hf})_{\text{Sample}}^0 \times (e^{AT} - 1)]/[(\text{176Hf}/\text{177Hf})_{\text{CHUR}}^0 - (\text{176Lu}/\text{177Hf})_{\text{CHUR}}^0 \times (e^{AT} - 1)]\} - 1\} \times 10^4$ .
$T_{\text{DM}} = 1/\lambda \times \ln \{1 + [((\text{176Hf}/\text{177Hf})_{\text{Sample}}^0 - (\text{176Hf}/\text{177Hf})_{\text{DM}}^0)/((\text{176Lu}/\text{177Hf})_{\text{Sample}}^0 - (\text{176Lu}/\text{177Hf})_{\text{DM}}^0)]\}$ .
$T_{\text{DM}}^{\text{C}} = T_{\text{DM}} - (T_{\text{DM}} - t) \times [(f_{\text{CC}} - f_{\text{S}})/(f_{\text{CC}} - f_{\text{DM}})]$ .
$f_{\text{Lu/Hf}} = [(\text{176Lu}/\text{177Hf})_{\text{Source}}/(\text{176Lu}/\text{177Hf})_{\text{CHUR}}, 0] - 1$ .
$(\text{176Lu}/\text{177Hf})_{\text{CHUR}, 0} = 0.0332 \pm 2$ .
$(\text{176Hf}/\text{177Hf})_{\text{CHUR}, 0} = 0.282772 \pm 29$ .
$(\text{176Lu}/\text{177Hf})_{\text{DM}} = 0.0384$ .
$(\text{176Hf}/\text{177Hf})_{\text{DM}} = 0.28325$ .
$(\text{176Lu}/\text{177Hf})_{\text{mean crust}} = 0.015$ .
$f_{\text{CC}} = (0.015/0.0332) - 1 = -0.5482$ .
$f_{\text{DM}} = (0.0384/0.0332) - 1 = 0.1566$ .

<sup>a</sup> U-Pb and Lu-Hf isotopic results from Liang et al. (2008).

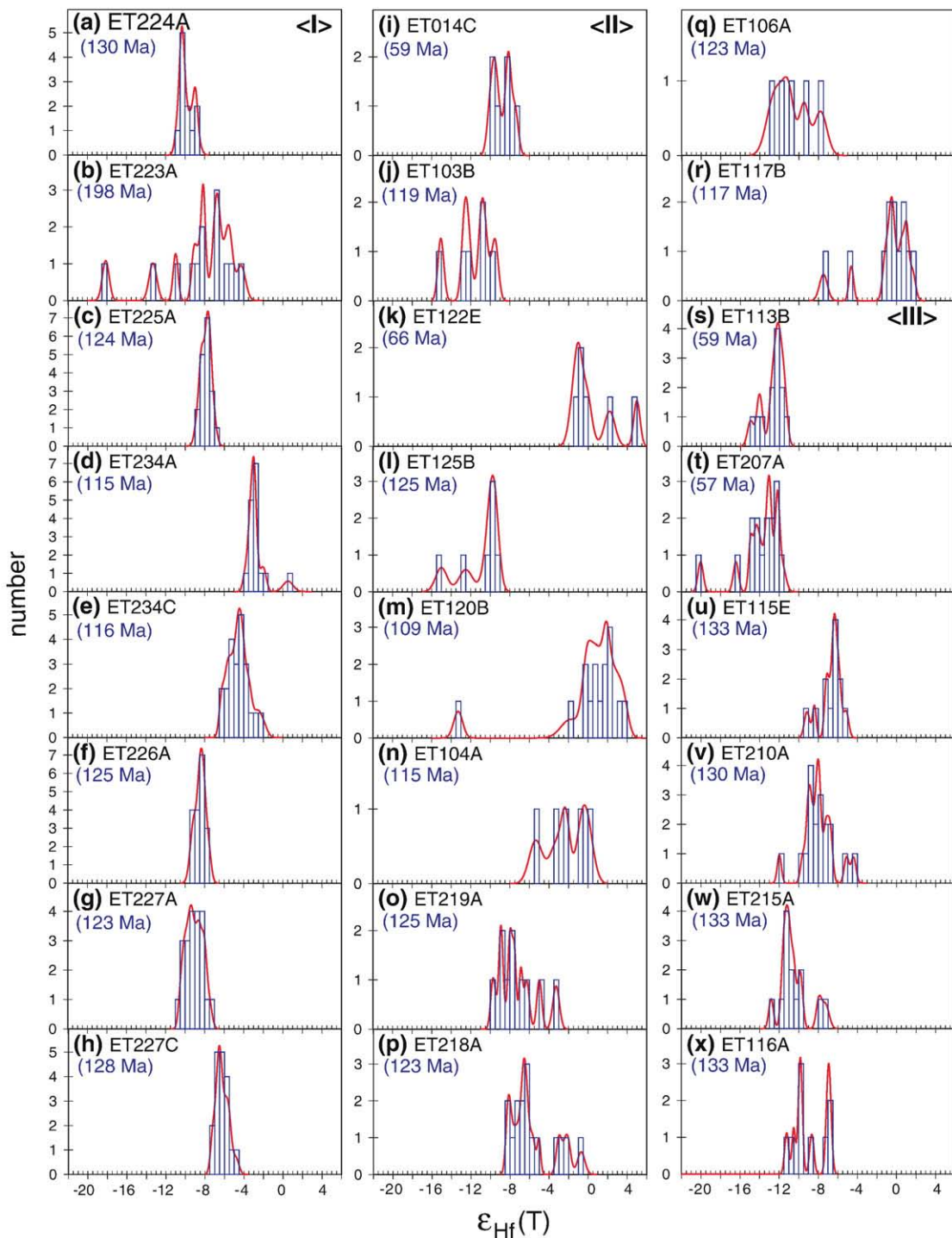


**Fig. 6.** Histograms of  $\epsilon_{\text{Hf}}(T)$  values of the eastern Himalayan batholiths. Note that the symbols <I>, <II> and <III> denote the Basu–Ranwu, Bomi–Ranwu and Chayu–Shama batholiths, respectively.

Indian border and inaccessible for study. However, our ongoing work on riverbank sediments from the Lohit River ( $\sim 96.2^\circ\text{E}/27.9^\circ\text{N}$ ) identifies abundant Gangdese-type zircons aged  $\sim 100$ – $120$  Ma coupled with high, positive  $\epsilon_{\text{Hf}}(T)$  values of  $\sim 15$  (Liang et al., unpubl. data), supporting the existence of Gangdese like igneous bodies in the upper reaches of the drainage.

While a general consensus has been reached for generating the Gangdese magmatism by the Neo-Tethyan northward subduction underneath the Lhasa terrane, the petrogenesis of the northern plutonic belt remains controversial. Through a comparative analysis, Xu et al. (2009) recently pointed out that the Cretaceous granitoids in

the northern plutonic belt show overall geochemical similarities to the North American Cordilleran Interior batholiths that did not form directly in a subduction setting but resulted from an intracontinental collisional setting, in which magma generation took place in response to crustal thickening followed in some cases by extension (cf. Driver et al., 2000). Therefore, Xu et al. (2009), adopting the view of Pearce and Mei (1988), argued that the northern plutonic belt was formed in a postcollisional regime in response to the Late Jurassic–Early Cretaceous collision between the Qiangtang and Lhasa terranes, and that the S-type magmatism was initiated as a result of significant crustal thickening, which may have capabilities of causing crustal

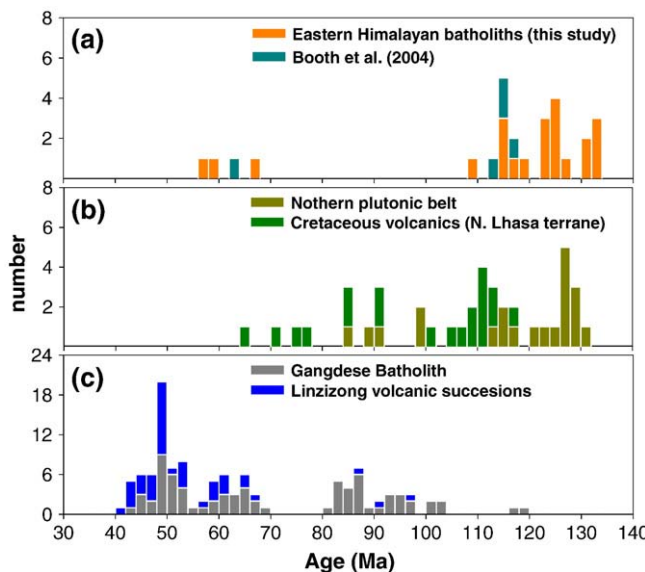


**Fig. 7.** Histograms of compiled crystallization ages of (a) the eastern Himalayan batholiths, (b) intrusive and volcanic rocks in the northern Lhasa terrane (data sources include Wen et al., 2008a; Lee et al., this volume; and references therein) and (c) the Gangdese Batholith (Wen et al., 2008a) and the Linzizong volcanic rocks (Lee et al., this volume) in the southern Lhasa terrane.

anatexis by itself. The evidence for regional crustal thickening has been reported by Kapp et al. (2005a), which estimated a >50% shortening, and thus thickening, in the continental crust of the northern Lhasa terrane occurring prior to the India–Asia collision.

However, the postcollisional scenario cannot accommodate the Early Jurassic magmatism in the eastern Himalayan batholiths, and may even hardly account for the generation of Early to Late Jurassic S-type granitoids in the Nyainqntanglha Range and other localities in the west (Fig. 10). The S-type magmatism, though most active in the Early Cretaceous, lasted until Late Cretaceous and Paleocene time (Fig. 7a and b). Such an igneous longevity implies a longer-lasting mechanism, as exemplified by the Cordilleran orogeny in the Central

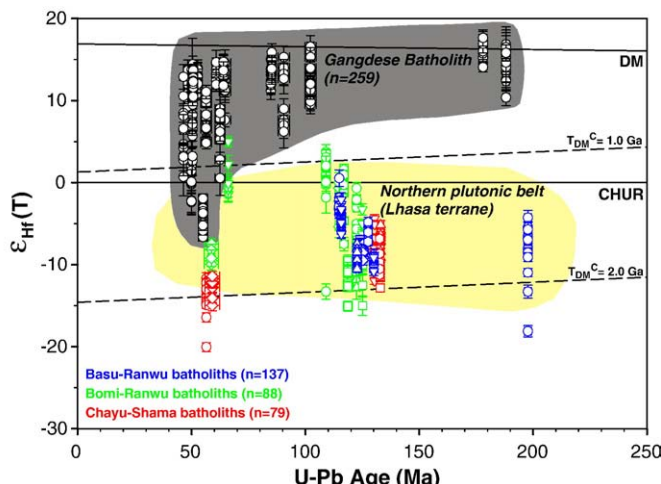


**Fig. 8.** Plots of  $\varepsilon_{\text{Hf}}(T)$  values versus U-Pb ages of magmatic zircons from eastern Himalayan batholiths. For comparison, available magmatic zircon data of the Gangdese Batholith are also plotted (Chu, 2006; Chu et al., 2006; Lee et al., 2007; Zhang et al., 2007a). Fields of the Gangdese Batholith (grey field) and northern plutonic belt (yellow field) are after Chu (2006) and Chu et al. (2006).  $2\sigma$  analytical errors of individual data points are given. CHUR—chondritic uniform reservoir; DM—depleted mantle. See Table 3 for notations of  $\varepsilon_{\text{Hf}}(T)$ , and the CHUR and DM evolutionary curves. (For interpretation of the references to colour in this figure legend, the reader is referred to the web version of this article.)

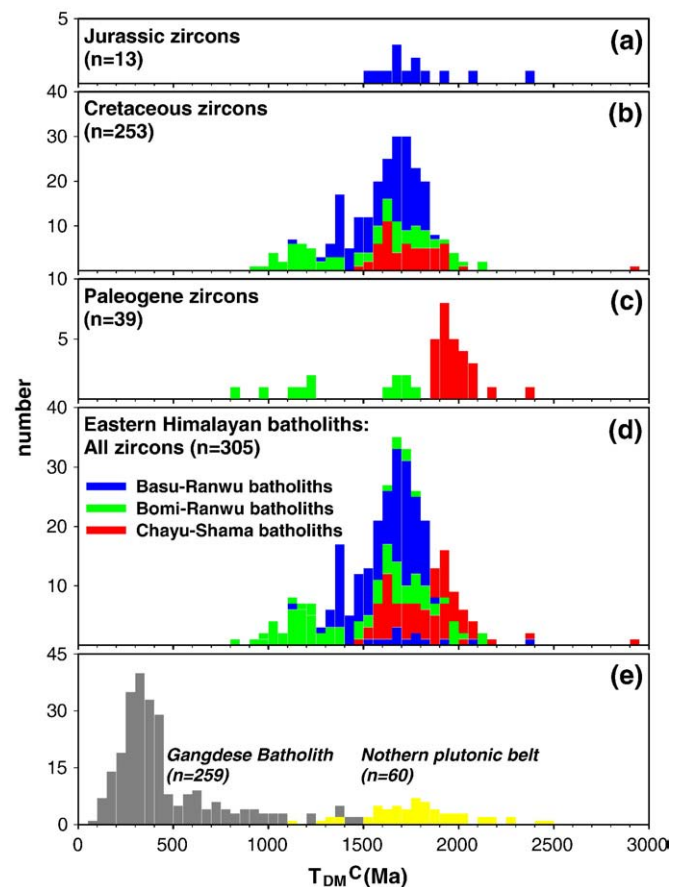


**Fig. 9.** Histograms of zircon  $T_{\text{DM}}^{\text{C}}$  (zircon Hf isotope crustal model age) results of (a) Jurassic, (b) Cretaceous, and (c) Paleogene granitoids from the eastern Himalayan batholiths. Note that sample ET122A aged ~66 Ma is plotted in (c). In (d), all zircon data ( $n = 305$ ) reported in this study are piled up. In (e), zircon  $T_{\text{DM}}^{\text{C}}$  results of the Gangdese Batholith (grey bars; Chu, 2006; Chu et al., 2006; Lee et al., 2007; Zhang et al., 2007a) and northern plutonic belt (yellow bars; Chu et al., 2006) are also plotted for comparison. Calculation details regarding  $T_{\text{DM}}^{\text{C}}$  ages are given in Table 3. (For interpretation of the references to colour in this figure legend, the reader is referred to the web version of this article.)

Andes (e.g., Allmendinger et al., 1997) and western North America (e.g., Wells and Hoisch, 2008). By analogy, the northward Neo-Tethyan subduction, rather than the postcollisional tectonic process that would often be relatively shorter-lived, is suggested to have played a role in the magmatism. Therefore, while we agree that generation of the widespread Early Cretaceous granitoids in the northern plutonic belt and eastern Himalayan batholiths is perhaps best interpreted as in response to collision-induced crustal thickening, continued or recurrent “far-field” interplays with the Neo-Tethyan subduction related processes, such as back-arc extension (Zhang et al., 2004; Wen et al., 2008a), should have also played a crucial and long-lived role since the Early Jurassic in the petrogenesis of the entire region.

## 6. Concluding remarks

- (1) Zircon U-Pb dating results of the eastern Himalayan batholiths indicate that the intrusive bodies were emplaced principally in the Early Cretaceous (~133–110 Ma) and subordinately in the Paleocene (~66–57 Ma), long after an older granite intrusion that also occurred in the region in the earliest Jurassic (~198 Ma).
- (2) These zircons have  $\varepsilon_{\text{Hf}}(T)$  values from +5 to –20, which yield Hf crustal model ages from 0.8 to 2.4 Ga, peaking ~1.7 Ga, thereby suggesting a major episode of crustal growth in the

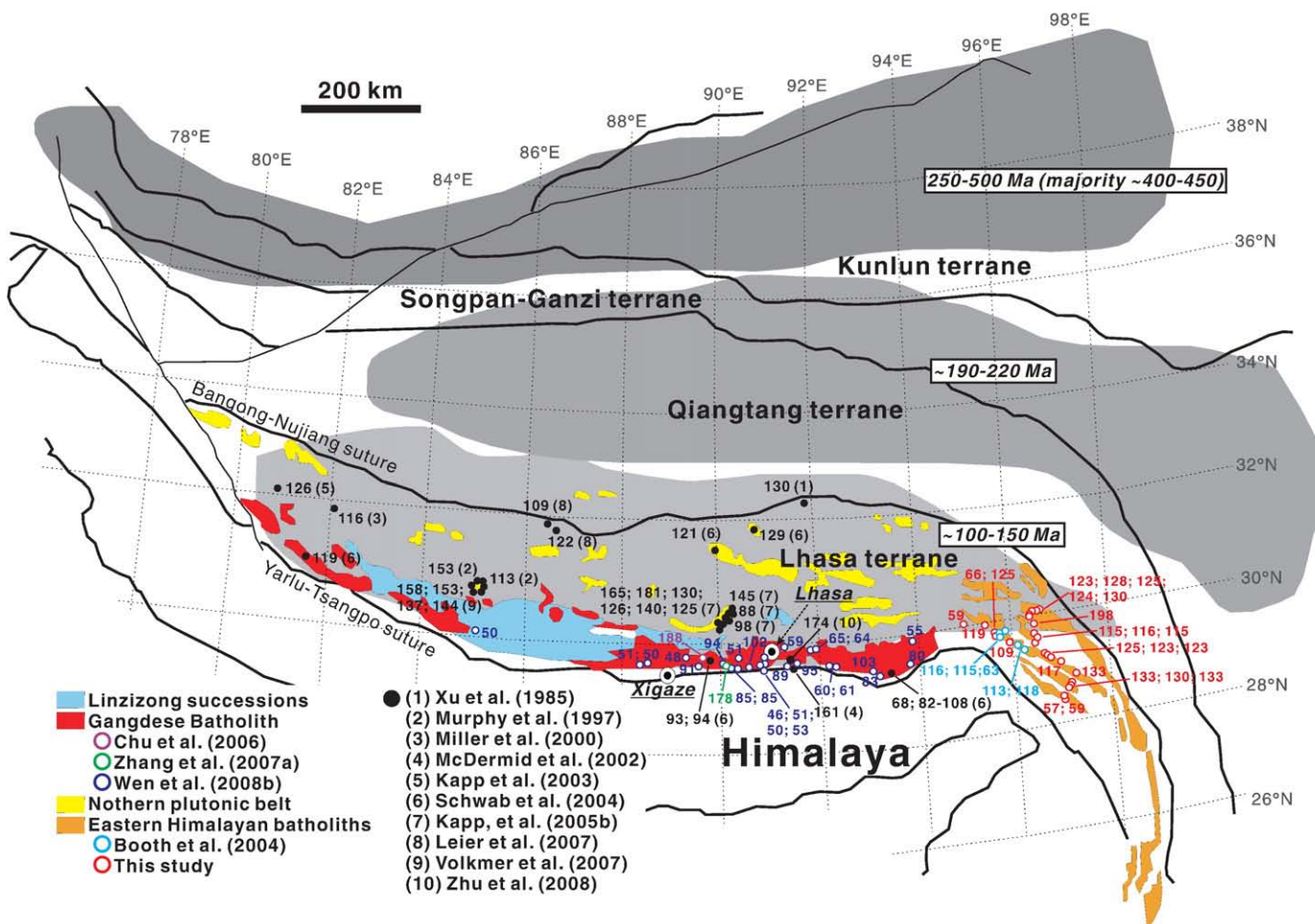


**Fig. 10.** Zircon U-Pb ages of Mesozoic to Paleogene igneous rocks in the Lhasa terrane, southern Tibet. Ages are given in Ma and the corresponding reference is denoted by the number in parentheses. The data sources include Kapp et al. (2003), McDermid et al. (2002), Miller et al. (2000), Murphy et al. (1997), Schwab et al. (2004) and Volkmer et al. (2007), not being cited for discussion in the text. The shaded regions are adopted from Leier et al. (2007) that highlighted general magmatic evolutionary trends in the Tibetan plateau.

Proterozoic and a predominantly crustal source involved in the granitoid petrogenesis in the eastern Himalayan batholiths.

- (3) The combined zircon U-Pb and Hf isotopic data, together with whole-rock geochemical information, allow us to correlate the eastern Himalayan batholiths to S-type granitoids in the northern plutonic belt of the Lhasa terrane, rather than to the I-type Gangdese Batholith from the central part of the southern Lhasa terrane.
- (4) The Early Cretaceous granitoids emplaced widely in the northern plutonic belt and eastern Himalayan batholiths were probably generated in a postcollisional regime in response to the Late Jurassic–Early Cretaceous collision between the Qiangtang and Lhasa terranes. If so, the widespread S-type magmatism was initiated as a result of significant collision-induced crustal thickening, a process that may have been capable by itself of causing regional crustal melting. However, the existence of Early Jurassic and Late Cretaceous–Paleocene S-type granitoids, though less abundant, implies that a longer-lived tectonic process related more likely to the Neo-Tethyan subduction may have also played a crucial role since the Early Jurassic in the petrogenesis of the entire region.

Science Council, Taiwan, ROC. Setup of the LA-ICPMS Lab at NTU was helped at various stages by W.L. Griffin, X.-H. Li, X.-R. Liang, N.J. Norman, and J.-H. Yang. We acknowledge two anonymous journal reviewers for their constructive comments that helped improve the paper.

## References

- Allègre, C.J., et al., 1984. Structure and evolution of the Himalaya-Tibet orogenic belt. *Nature* 307, 17–22.
- Allmendinger, R.W., Jordan, T.E., Kay, S.M., Isacks, B.L., 1997. The evolution of the Altiplano-Puna Plateau of the Central Andes. *Ann. Rev. Earth Planet. Sci.* 25, 139–174.
- Anderson, T., 2002. Correction of common lead in U-Pb analyses that do not report  $^{204}\text{Pb}$ . *Pb. Chem. Geol.* 192, 59–79.
- Black, L.P., Gulson, B.L., 1978. The age of the Mud Tank carbonatite, Strangways Range, Northern Territory. *BMR J. Aust. Geol. Geophys.* 3, 227–232.
- Booth, A.L., Zeitler, P.K., Kidd, W.S.F., Wooden, J., Liu, Y., Idleman, B., Hren, M., Chamberlain, C.P., 2004. U-Pb zircon constraints on tectonic evolution of southeastern Tibet, Namche Barwa area. *Am. J. Sci.* 304, 889–929.
- Chang, C., et al., 1986. Preliminary conclusions of the Royal Society and Academia Sinica 1985 geotraverse of Tibet. *Nature* 323, 501–507.
- Chu, M.-F., 2006. Application of ICP-MS to the Study of Transhimalayan Petrogenesis. Ph. D. thesis, National Taiwan University.
- Chu, M.-F., Chung, S.-L., Song, B., Liu, D., O'Reilly, S.Y., Pearson, N.J., Ji, J., Wen, D.-J., 2006. Zircon U-Pb and Hf isotope constraints on the Mesozoic tectonics and crustal evolution of southern Tibet. *Geology* 34, 745–748.
- Chu, M.-F., Chung, S.-L., O'Reilly, S.Y., Pearson, N.J., Wu, F.-Y., Li, X.-H., Liu, D., Ji, J., Chu, C.-H., Gallet, S., in press. Tibetan orogeny with India's hidden inputs revealed by Hf isotopes of Transhimalayan zircons and host rocks.
- Chung, S.-L., Liu, D., Ji, J., Chu, M.-F., Lee, H.-Y., Wen, D.-J., Lo, C.-H., Lee, T.-Y., Qian, Q., Zhang, Q., 2003. Adakites from continental collision zones: melting of thickened lower crust beneath southern Tibet. *Geology* 31, 1021–1024.

## Acknowledgments

We thank H.-Y. Lee, J. Ji and Mary Yeh for their help in the field, H. Tao for zircon preparation, and Y.-G. Xu for sharing ideas during this study, which benefited from financial supports to SLC by the National

- Chung, S.-L., Chu, M.-F., Zhang, Y., Xie, Y., Lo, C.-H., Lee, T.-Y., Lan, C.-Y., Li, X., Zhang, Q., Wang, Y., 2005. Tibetan tectonic evolution inferred from spatial and temporal variations in post-collisional magmatism. *Earth-Sci. Rev.* 68, 173–196.
- Coulon, C., Maluski, H., Bollinger, C., Wang, S., 1986. Mesozoic and Cenozoic volcanic rocks from central and southern Tibet:  $^{39}\text{Ar}$ – $^{40}\text{Ar}$  dating, petrological characteristics and geodynamical significance. *Earth Planet. Sci. Lett.* 79, 281–302.
- Debon, F., Le Fort, P., Sheppard, S.M.F., Sonet, J., 1986. The four plutonic belts of the Transhimalaya-Himalaya: a chemical, mineralogical, isotopic, and chronological synthesis along a Tibet-Nepal section. *J. Petrol.* 27, 219–250.
- Ding, L., Kapp, P., Zhong, D., Deng, W., 2003. Cenozoic volcanism in Tibet: evidence from a transition from oceanic to continental subduction. *J. Petrol.* 44, 1833–1865.
- Driver, L.A., Creaser, R.A., Chacko, T., Erdmer, P., 2000. Petrogenesis of the Cretaceous Cassiar batholith, Yukon-British Columbia, Canada: implications for magmatism in the North American Cordilleran Interior. *Bull. Geol. Soc. Am.* 112, 1119–1133.
- Eggins, S.M., Kinsley, L.P.J., Shelley, J.M.G., 1998. Deposition and element fractionation processes during atmospheric pressure laser sampling for analysis by ICP-MS. *Appl. Surf. Sci.* 127–129, 278–286.
- Griffin, W.L., Wang, X., Jackson, S.E., Pearson, N.J., O'Reilly, S.Y., Xu, X., Zhou, X., 2002. Zircon chemistry and magma mixing, SE China: in-situ analysis of Hf isotopes, Tonglu and Pingtan igneous complexes. *Lithos* 61, 237–269.
- Günther, D., Heinrich, C.A., 1999. Enhanced sensitivity in laser ablation-ICP mass spectrometry using helium–argon mixtures as aerosol carrier. *J. Anal. At. Spectrom.* 14, 1363–1368.
- Harris, N.B.W., Xu, R.H., Lewis, C.L., Jin, C., 1988. Plutonic rocks of the 1985 Tibet Geotransverse: Lhasa to Golmud. *Philos. Trans. R. Soc. Lond.* A327, 263–285.
- Harris, N.B.W., Inger, S., Xu, R., 1990. Cretaceous plutonism in Central Tibet: an example of post-collision magmatism? *J. Volcanol. Geotherm. Res.* 44, 21–32.
- Hoskin, P.W.O., Schaltegger, U., 2003. The Composition of Zircon and Igneous and Metamorphic Petrogenesis. In: Manchar, J.M., Hoskin, P.W.O. (Eds.), *Zircon, Reviews of Mineralogy and Geochemistry*, vol. 53, pp. 27–62.
- Ireland, T.R., Williams, I.S., 2003. Considerations in Zircon geochronology by SIMS. In: Manchar, J.M., Hoskin, P.W.O. (Eds.), *Zircon, Reviews of Mineralogy and Geochemistry*, vol. 53, pp. 215–241.
- Jackson, S.E., Pearson, N.J., Griffin, W.L., Belousova, E.A., 2004. The application of laser ablation-inductively coupled plasma-mass spectrometry to in situ U-Pb zircon geochronology. *Chem. Geol.* 211, 47–69.
- Kapp, P., Yin, A., Manning, C.E., Harrison, T.M., Taylor, M.H., 2003. Tectonic evolution of the early Mesozoic blueschist-bearing Qiangtang metamorphic belt, central Tibet. *Tectonics* 22, 1043.
- Kapp, P., Yin, A., Harrison, T.M., Ding, L., 2005a. Cretaceous–Tertiary shortening, basin development, and volcanism in central Tibet. *Geol. Soc. Amer. Bull.* 117, 865–878.
- Kapp, J.L.D., Harrison, T.M., Kapp, P., Grove, M., Lovera, O.M., Ding, L., 2005b. Nyainqntanglha Shan: a window into the tectonic, thermal, and geochemical evolution of the Lhasa block, southern Tibet. *J. Geophys. Res.* 110, B08413.
- Lee, H.-Y., Chung, S.-L., Wang, Y., Zhu, D., Yang, J., Song, B., Liu, D., Wu, F.-Y., 2007. Age, petrogenesis and geological significance of the Linzizong volcanic successions in the Linzizong basin, southern Tibet: evidence from zircon U-Pb dates and Hf isotopes. *Acta Petrol. Sin.* 23, 493–500.
- Lee, H.-Y., Chung, S.-L., Lo, C.-H., Ji, J., Lee, T.-Y., Qian, Q., Zhang, Q., this volume. Eocene Neotethyan slab breakoff in southern Tibet inferred from the Linzizong volcanic record. *Tectonophysics*.
- Leier, A.L., Kapp, P., Gehrels, G.E., DeCelles, P.G., 2007. Detrital zircon geochronology of Carboniferous–Cretaceous strata in the Lhasa terrane, Southern Tibet. *Basin Res.* 19, 361–378.
- Liang, Y.-H., Chung, S.-L., Liu, D., O'Reilly, S.Y., Chu, M.-F., Ji, J., Song, B., Pearson, N.J., 2004. Detrital zircon study along the Tsangpo River, SE Tibet. *Eos Trans. AGU* 85 (47), Fall Meeting Abstract T53A-0466.
- Liang, Y.-H., Chung, S.-L., Liu, D., Xu, Y., Wu, F.-Y., Yang, J.-H., Wang, Y., Lo, C.-H., 2008. Detrital zircon evidence from Burma for reorganization of the eastern Himalayan river system. *Am. J. Sci.* 308, 618–638.
- Lin, I.-J., 2007. Geochemical Constraints on the Petrogenesis of Cretaceous to Paleocene Granitoids and Volcanic Rocks from SE Tibet. MSc Thesis, National Taiwan University.
- Lin, I.-J., Chung, S.-L., Chu, C.-H., Gallet, S., Ji, J., 2007. The petrogenesis of Cretaceous A-type granites, SE Tibet: geochemical and Nd isotopic constraints. *Eos Trans. AGU* 88 (52), Fall Meeting Abstract T31B-0468.
- Ludwig, K.R., 2003. Isoplot v. 3.0: A Geochronological Toolkit for Microsoft Excel. Special Publication, No. 4. Berkeley Geochronology Center. 70 pp.
- McDermid, I.R.C., Aitchison, J.C., Davis, A.M., Harrison, T.M., Grove, M., 2002. The Zedong terrane: a Late Jurassic intra-oceanic magmatic arc within the Yarlung-Tsangpo suture zone, southeastern Tibet. *Chem. Geol.* 187, 267–277.
- Miller, C., Schuster, R., Kotzli, U., Frank, W., Grasemann, B., 2000. Late Cretaceous–Tertiary magmatic and tectonic events in the Transhimalayan batholith (Kailas area, SW Tibet). *Schweiz. Mineral. Petrol.* 80, 1–20.
- Mo, X.X., Dong, G., Zhao, Z., Zhou, S., Wang, L., Qiu, R., Zhang, F., 2005. Spatial and temporal distribution and characteristics of granitoids in the Gangdese, Tibet and implication for crustal growth and evolution. *Geol. J. Chinese University* 11, 281–190.
- Mo, X.X., Hou, Z., Niu, Y., Dong, G., Qu, X., Zhao, Z., Yang, Z., 2007. Mantle contributions to crustal thickening during continental collision: evidence from Cenozoic igneous rocks in southern Tibet. *Lithos* 96, 225–242.
- Murphy, M.A., Yin, A., Harrison, T.M., Dürr, S.B., Chen, Z., Ryerson, F.J., Kidd, W.S.F., Wang, X., Zhou, X., 1997. Did the Indo-Asian collision alone create the Tibetan Plateau? *Geology* 25, 719–722.
- Pan, G., Ding, J., Yao, D., Wang, L., chief compilers, 2004. Guidebook of 1:1,500,000 geologic map of the Qinghai-Xizang (Tibet) plateau and adjacent areas. Chengdu Cartographic Publ. House, Chengdu, China. 48 p.
- Pearce, J.A., Mei, H., 1988. Volcanic rocks of the 1985 Tibet Geotraverse: Lhasa to Golmud. *Philos. Trans. R. Soc. Lond.* A327, 169–201.
- Scherer, E., Münker, C., Mezger, K., 2001. Calibration of the lutetium-hafnium clock. *Science* 293, 683–687.
- Schwab, M., Ratschbacher, L., Siebel, W., McWilliams, M., Minaev, V., Lutkov, V., Chen, F., Stanek, K., Nelson, B., Frisch, W., Wooden, J.L., 2004. Assembly of the Pamirs: age and origin of magmatic belts from southern Tien Shan to the southern Pamirs and their relation to Tibet. *Tectonics* 23, TC4002.
- Searle, M.P., Windley, B.F., Coward, M.P., Cooper, D.J.W., Rex, D., Li, T., Xiao, X., Jan, M.Q., Thakur, V.C., Kumar, S., 1987. The closing of Tethys and the tectonics of Himalaya. *Geol. Soc. Amer. Bull.* 98, 678–701.
- Tu, G., Zhang, Y., Wang, Z., 1982. *Geochemistry of Granitoids in Southern Xizang (Tibet)*. Sci. Publ. House, Beijing. 190 pp. (in Chinese).
- Volkmer, J.B., Kapp, P., Guynn, J.H., Lai, Q., 2007. Cretaceous–Tertiary evolution of the north central Lhasa terrane, Tibet. *Tectonics* 26, TC6007.
- Wells, M.L., Hoisch, T.D., 2008. The role of mantle delamination in widespread Late Cretaceous extension and magmatism in the Cordilleran orogen, western United States. *Bull. Geol. Soc. Am.* 120, 515–530.
- Wen, D.-R., Liu, D., Chung, S.-L., Chu, M.-F., Ji, J., Zhang, Q., Song, B., Lee, T.-Y., Yeh, M.-W., Lo, C.-H., 2008a. Zircon SHRIMP U-Pb ages of the Gangdese Batholith and implications for Neotethyan subduction in southern Tibet. *Chem. Geol.* 252, 191–201.
- Wen, D.-R., Chung, S.-L., Song, B., Izuka, Y., Yang, H.-J., Ji, J., Liu, D., Gallet, S., 2008b. Late Cretaceous Gangdese intrusions of adakitic geochemical characteristics, SE Tibet: petrogenesis and tectonic implications. *Lithos* 105, 1–11.
- Wiendebrock, M., Allé, P., Corfu, F., Griffin, W.L., Meier, M., Oberli, F., Von Quadt, A., Roddick, J.C., Spiegel, W., 1995. Three natural zircon standards for U-Th-Pb, Lu-Hf, trace element and REE analyses. *Geostand. Newslett.* 19, 1–23.
- Wu, F.-Y., Yang, Y.-H., Xie, L.-W., Yang, J.-H., Xu, P., 2006. Hf isotopic compositions of the standard zircons and baddeleyites used in U-Pb geochronology. *Chem. Geol.* 234, 105–126.
- Wu, F.-Y., Ji, W.-Q., Liu, C.-Z., Chung, S.-L., 2009. Detrital zircon U-Pb and Hf isotopic constraints from the Xigaze fore-arc basin, southern Tibet on the source provenance and Transhimalayan magmatic evolution. *J. Geophys. Res.* in revision.
- Xu, R., Scharer, U., Allègre, C.J., 1985. Magmatism and metamorphism in the Lhasa Block (Tibet): a geochronological study. *J. Geol.* 93, 41–57.
- Xu, Y.-G., Yang, Q.-J., Lan, J.-B., Huang, X.-L., Luo, Z.-Y., Shi, Y.-R., Xie, L.-W., 2009. Zircon U-Pb age and Hf isotopes of batholiths in the Gaoligong–Tengliang belt, eastern Tibet: a comparison with the Lhasa terrane and tectonic implications. *J. Geophys. Res.* in revision.
- Yin, A., Harrison, T.M., 2000. Geologic evolution of the Himalayan-Tibetan orogen. *Ann. Rev. Earth Planet. Sci.* 28, 211–280.
- Zhang, K.J., Xia, B.D., Wang, G.M., Li, Y.T., Ye, H.F., 2004. Early Cretaceous stratigraphy, depositional environments, sandstone provenance, and tectonic setting of central Tibet, western China. *Geol. Soc. Am. Bull.* 116, 1202–1222.
- Zhang, H.F., Xu, W.C., Guo, J.Q., Zong, K.Q., Cai, H.M., Yuan, H.L., 2007a. Zircon U-Pb and Hf isotopic composition of deformed granite in the southern margin of the Gangdese belt, Tibet: evidence for early Jurassic subduction of Neo-Tethyan oceanic slab. *Acta Petrol. Sin.* 23, 1347–1353.
- Zhang, H.F., Xu, W.C., Guo, J.Q., Zong, K.Q., Cai, H.M., Yuan, H.L., 2007b. Indosian orogenesis of the Gangdese terrane: evidences from zircon U-Pb dating and petrogenesis of granitoids. *Earth Sci. J. China Univ. Geosci.* 32, 155–166.
- Zhu, D.-C., Pan, G., Chung, S.-L., Liao, Z., Wang, L., Li, G., 2008. SHRIMP zircon age and geochemical constraints on the origin of lower Jurassic volcanic rocks from the Yeba Formation, southern Gangdese, south Tibet. *Int. Geol. Rev.* 50, 442–471.